Promyelocytic Leukemia Protein (PML) Controls Listeria monocytogenes Infection.

David Ribet, Valérie Lallemand-Breitenbach, Omar Ferhi, Marie-Anne Nahori, Hugo Varet, Hugues de Thé, Pascale Cossart

AMERICAN SOCIETY FOR MICROBIOLOGY | mBio®

RESEARCH ARTICLE

Promyelocytic Leukemia Protein (PML) Controls *Listeria monocytogenes* Infection

David Ribet,[a,b,c] Valérie Lallemand-Breitenbach,[d,e] Omar Ferhi,[d,e] Marie-Anne Nahori,[a,b,c] Hugo Varet,[f,g] Hugues de Thé,[d,e] Pascale Cossart[a,b,c]

Institut Pasteur, Unité des Interactions Bactéries-Cellules, Paris, France[a]; Inserm, U604, Paris, France[b]; INRA, USC2020, Paris, France[c]; Inserm, CNRS, Université Paris Diderot, Institut Universitaire Hématologie, U944/UMR7212, Hôpital St. Louis, Paris, France[d]; PSL, Collège de France, Paris, France[e]; Institut Pasteur, Plateforme Transcriptome et Epigenome, Biomics, Centre d'Innovation et Recherche Technologique (Citech), Paris, France[f]; Institut Pasteur, Hub Bioinformatique et Biostatistique, Centre de Bioinformatique, Biostatistique et Biologie Intégrative (C3BI, USR 3756 IP CNRS), Paris, France[g]

ABSTRACT The promyelocytic leukemia protein (PML) is the main organizer of stress-responsive subnuclear structures called PML nuclear bodies. These structures recruit multiple interactors and modulate their abundance or their posttranslational modifications, notably by the SUMO ubiquitin-like modifiers. The involvement of PML in antiviral responses is well established. In contrast, the role of PML in bacterial infection remains poorly characterized. Here, we show that PML restricts infection by the pathogenic bacterium *Listeria monocytogenes* but not by *Salmonella enterica* serovar Typhimurium. During infection, PML undergoes oxidation-mediated multimerization, associates with the nuclear matrix, and becomes de-SUMOylated due to the pore-forming activity of the *Listeria* toxin listeriolysin O (LLO). These events trigger an antibacterial response that is not observed during *in vitro* infection by an LLO-defective *Listeria* mutant, but which can be phenocopied by specific induction of PML de-SUMOylation. Using transcriptomic and proteomic microarrays, we also characterized a network of immunity genes and cytokines, which are regulated by PML in response to *Listeria* infection but independently from the listeriolysin O toxin. Our study thus highlights two mechanistically distinct complementary roles of PML in host responses against bacterial infection.

IMPORTANCE The promyelocytic leukemia protein (PML) is a eukaryotic protein that can polymerize in discrete nuclear assemblies known as PML nuclear bodies (NBs) and plays essential roles in many different cellular processes. Key to its function, PML can be posttranslationally modified by SUMO, a ubiquitin-like modifier. Identification of the role of PML in antiviral defenses has been deeply documented. In contrast, the role of PML in antibacterial defenses remains elusive. Here, we identify two mechanistically distinct complementary roles of PML in antibacterial responses against pathogens such as *Listeria*: (i) we show that PML regulates the expression of immunity genes in response to bacterial infection, and (ii) we unveil the fact that modification of PML SUMOylation by bacterial pore-forming toxins is sensed as a danger signal, leading to a restriction of bacterial intracellular multiplication. Taken together, our data reinforce the concept that intranuclear bodies can dynamically regulate important processes, such as defense against invaders.

Received 6 December 2016 **Accepted** 8 December 2016 **Published** 10 January 2017

Citation Ribet D, Lallemand-Breitenbach V, Ferhi O, Nahori M-A, Varet H, de Thé H, Cossart P. 2017. Promyelocytic leukemia protein (PML) controls *Listeria monocytogenes* infection. mBio 8:e02179-16. https://doi.org/10.1128/mBio.02179-16.

Editor Arturo Casadevall, Johns Hopkins Bloomberg School of Public Health

Address correspondence to Hugues de Thé, hugues.dethe@inserm.fr, or Pascale Cossart, pascale.cossart@pasteur.fr.

Promyelocytic leukemia protein (PML) is a protein originally identified as part of a t(15:17) chromosomal translocation resulting in the fusion of *PML* and retinoic acid receptor alpha genes in acute promyelocytic leukemia (APL) patients (1–5). In normal cells, PML is present both as a diffuse form in the nucleoplasm and cytoplasm and polymerized in discrete subnuclear structures known as PML nuclear bodies (NBs). PML proteins define the boundaries of these NBs, which constitute non-membrane-bound

compartments in the nucleoplasm (6–8). PML NBs are dynamic stress-responsive structures that constitutively or transiently have the ability to recruit a large number of proteins. Studies investigating the basis for arsenic trioxide-initiated APL cure have suggested that oxidative stress promotes PML multimerization and PML NB formation (6, 7, 9–12). PML NBs may also regulate the posttranslational modifications of recruited proteins, thereby controlling their sequestration, activation, or stability (11–13). In agreement with its large and diverse repertoire of interacting partners, PML is involved in many different cellular processes, such as senescence, apoptosis, or antiviral defense (6, 7, 14–17). The role of PML in antiviral defense is illustrated by the higher sensitivity of PML knockout mice to different viruses (reviewed in reference 16). Many viruses counteract this PML antiviral activity by decreasing PML expression or stability or by altering PML NB integrity (16, 17).

Listeria monocytogenes is a Gram-positive bacterium that is responsible for the foodborne disease listeriosis. Although well adapted to survive extracellularly, this pathogen can also infect, survive, and replicate in the cytoplasm of both macrophages and nonprofessional phagocytic cells, such as epithelial cells (18). The numerous strategies employed by *Listeria* to interfere with host processes have raised this bacterium as one of the best model organisms for the study of bacterial pathogenesis and pathophysiology. Among the different cellular pathways subverted by *Listeria*, we have previously demonstrated that infection of cells by this bacterium was associated with an alteration of the host SUMOylome, i.e., the repertoire of proteins posttranslationally modified by the ubiquitin-like SUMO polypeptide (19, 20). Strikingly, pore formation at the level of the host plasma membrane by listeriolysin O (LLO), a toxin secreted by *Listeria*, triggers the degradation of Ubc9, the unique E2 enzyme of the SUMOylation machinery in humans (20). This degradation leads to an inhibition of *de novo* SUMOylations. De-SUMOylation reactions, catalyzed by the different SUMO isopeptidases of the host cell, then result in a rapid loss of SUMO conjugates. Several nuclear factors, including transcription factors, are de-SUMOylated in response to infection, explaining how host SUMOylome alteration during *Listeria* infection leads to host transcription modifications (21).

Interestingly, other bacterial pathogens were shown to manipulate host SUMOylation machinery during infection. Infection of HeLa cells with *Shigella flexneri*, a pathogen causing bacillary dysentery, leads to a decrease in Ubc9 level and a modification of host SUMOylated proteins (22, 23). Transcription factors involved in inflammatory responses, such as c-FOS, RXRα, and PPAR γ, for example, are de-SUMOylated in response to *Shigella* infection (23). In addition, SUMOylation was reported to restrain production of inflammatory cytokines by silencing *ifnb1* expression (24). Alteration of SUMOylation may thus contribute to the inflammatory response associated with *Shigella*. *Salmonella enterica* serovar Typhimurium, a bacterium responsible for gastroenteritis in humans, was also shown to decrease the Ubc9 level during infection and to alter the host SUMOylome during infection (25). Together, these studies unveiled the role of SUMOylation in the regulation of key host factors controlling infection by different classes of pathogens.

Interestingly, SUMOylation plays a critical role in the function of PML and PML NBs. PML can indeed be SUMOylated on several lysine residues, and PML SUMOylation is required for the recruitment of PML NB partners (26–33). In addition, most PML partners can be SUMOylated, and PML NBs are thought to facilitate this process through the recruitment of Ubc9 upon stress (11). Some of the PML partners are then degraded by SUMO-dependent ubiquitin ligases, such as RNF4 (34, 35). Thus, NBs couple stress to enhanced SUMOylation of PML interactors, enforcing multiple responses, such as TP53 activation, senescence, or antiviral effects (11, 13, 36).

In contrast to PML's established action against viruses, a single study mentioned that PML knockout mice are more sensitive to infection by *Listeria monocytogenes* (37). However, the exact role of PML in anti-*Listeria* responses or in other bacterial infections has not been elucidated. In this study, we demonstrate that PML restricts *Listeria* infection both *in vitro* and *in vivo*. We identify in particular that PML upregulates several

genes and cytokines involved in innate immunity. Moreover, in response to LLO-producing *Listeria*, PML multimerizes, associates with the nuclear matrix, and becomes de-SUMOylated, which ultimately impairs *Listeria* replication. Taken together, our data highlight different roles of PML in antibacterial responses, notably the role for PML's SUMOylation status in the sensing of and defense against bacterial pathogens that produce pore-forming toxins. Our findings further illustrate the concept that intranuclear bodies dynamically regulate important processes, such as defense against invaders.

RESULTS

Depletion of PML increases *Listeria* infection. In order to characterize the role of PML during infection *in vivo*, we first infected wild-type (WT) and PML knockout mice with *Listeria* (EGD strain). As mice are poorly permissive for oral infections with *Listeria*, due to lack of recognition of murine E-cadherin by the essential *Listeria* internalin A surface protein (InlA) (38), we used the intravenous route to perform infections. We enumerated CFUs (colony-forming units) in the liver and spleen of animals 3 days after infection (Fig. 1A). We observed a significantly higher number of CFUs per organ in $pml^{-/-}$ mice than in $pml^{+/+}$ mice, confirming that $pml^{-/-}$ mice are more sensitive to *Listeria* infection (37). We then similarly challenged $pml^{+/+}$ and $pml^{-/-}$ mice with *Salmonella* Typhimurium. In contrast to our observations with *Listeria*, we did not observe a significant difference in the number of CFUs per organ between wild-type and PML-deficient mice, thus revealing a specific defect of $pml^{-/-}$ mice in their responses against *Listeria* compared to their responses against another intracellular pathogen (Fig. 1B).

In order to further characterize the role of PML in bacterial infection, we then compared the infection efficiencies of *Listeria* (EGD strain) in immortalized mouse embryonic fibroblasts (MEFs) derived from $pml^{+/+}$ or $pml^{-/-}$ mice. The numbers of intracellular *Listeria* bacteria were quantified after 1.5 h, 5 h, and 24 h of infection (Fig. 1C). We did not observe significant differences in bacterial numbers after 1.5 h of infection, suggesting that the internalization efficiencies of *Listeria* are similar in $pml^{+/+}$ and $pml^{-/-}$ MEFs (see Fig. S1A in the supplemental material). In contrast, the number of intracellular bacteria after 24 h of infection was significantly higher in $pml^{-/-}$ than in $pml^{+/+}$ MEFs (Fig. 1C). These data indicate that *Listeria*'s intracellular replication is facilitated in the absence of PML in MEFs, thus demonstrating that PML restricts the bacterial replication in nonphagocytic cells. In parallel, we infected MEFs with another strain of *Listeria*, EGDe.PrfA* (an EGD-e strain in which PrfA, the master regulator of *Listeria* virulence genes, is constitutively active [39]). A significant increase in the number of intracellular CFUs was again observed in $pml^{-/-}$ MEFs compared to the number in $pml^{+/+}$ MEFs, confirming the role of PML in the control of *Listeria* infection (see Fig. S1B). Interestingly, infection of MEFs with *Salmonella* did not show significant differences in bacterial numbers at 1.5 h, 5 h, or 24 h, indicating that $pml^{+/+}$ and $pml^{-/-}$ MEFs are similarly sensitive to *Salmonella* entry and replication and thereby confirming our *in vivo* data and PML's specificity toward *Listeria* (Fig. 1C; see also Fig. S1A). Together, these data highlight that PML specifically restricts *Listeria* infection both *in vitro* and *in vivo*.

PML regulates the expression of genes involved in innate immunity. To better characterize the role of PML during bacterial infection, we compared gene expression and cytokine production in $pml^{+/+}$ and $pml^{-/-}$ MEFs after 24 h of infection with *Listeria* (EGD strain). RNAs extracted from infected MEFs were analyzed to profile the expression of 84 genes involved in the innate immune response using transcriptomic microarrays. We could identify 27 genes, including *camp*, *casp1*, *ccl3*, *cxcl1*, *irf7*, *lcn2*, *nlrp3*, *nod2*, *ripk2*, and *tlr2*, that were differentially expressed in $pml^{+/+}$ versus $pml^{-/-}$ MEFs following infection (Fig. 2; see also Table S1A in the supplemental material). This indicates that PML plays an important role in the regulation of these genes. We conducted a similar approach to identify putative PML-regulated cytokines. We collected supernatants from control and 24-h-infected $pml^{+/+}$ and $pml^{-/-}$ MEFs and

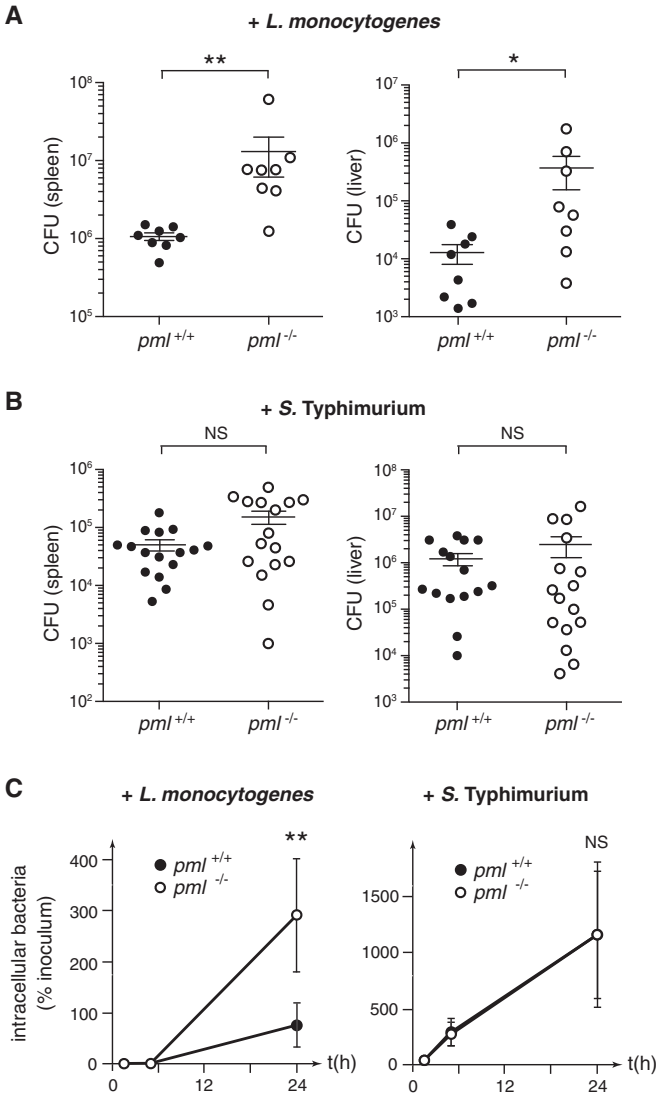

FIG 1 PML restricts *Listeria* infection. (A and B) $pml^{+/+}$ and $pml^{-/-}$ mice were infected with *L. monocytogenes* (A) or *S.* Typhimurium (B), and the numbers of CFUs per spleen and liver were quantified 72 h after infection (bars and whiskers show mean results ± standard errors of the means [SEM]; *, $P < 0.05$; **, $P < 0.01$; NS, not significant; Mann-Whitney statistical test). (C) $pml^{+/+}$ or $pml^{-/-}$ MEFs were infected with *L. monocytogenes* or *S.* Typhimurium, and the numbers of intracellular bacteria, represented as the percentages of the inoculum used for infection, were quantified (mean results ± SEM from 6 to 8 independent experiments; **, $P < 0.01$; NS, not significant; unpaired two-tailed Student's *t* test).

monitored the presence of 110 different cytokines using proteome microarrays. Again, we could identify 13 cytokines that were expressed in a PML-dependent manner (Fig. 2; see also Table S2A). Among these PML-regulated cytokines, we identified in particular *ccl20* and *cx3cl1*, 2 cytokines known to play key roles in antibacterial responses.

As LLO was shown to be a major determinant of host response to infection (40), we tested whether some of these PML-regulated genes or cytokines were expressed in an LLO-dependent manner. To do so, we analyzed $pml^{+/+}$ and $pml^{-/-}$ MEFs infected with an LLO-defective *Listeria* mutant (*Listeria* Δ*hly*). We observed that all genes and cytokines differentially regulated by PML in cells infected with wild-type bacteria were also differentially regulated in response to the Δ*hly Listeria* mutant (Fig. 2; see also Tables S1B and S2B). Thus, the PML-regulated genes and cytokines identified here are expressed in an LLO-independent manner. We finally monitored gene expression, using the same transcriptomic microarrays, in $pml^{+/+}$ MEFs treated or not with purified LLO. No gene from the 27 targets identified as being regulated by PML during wild-type

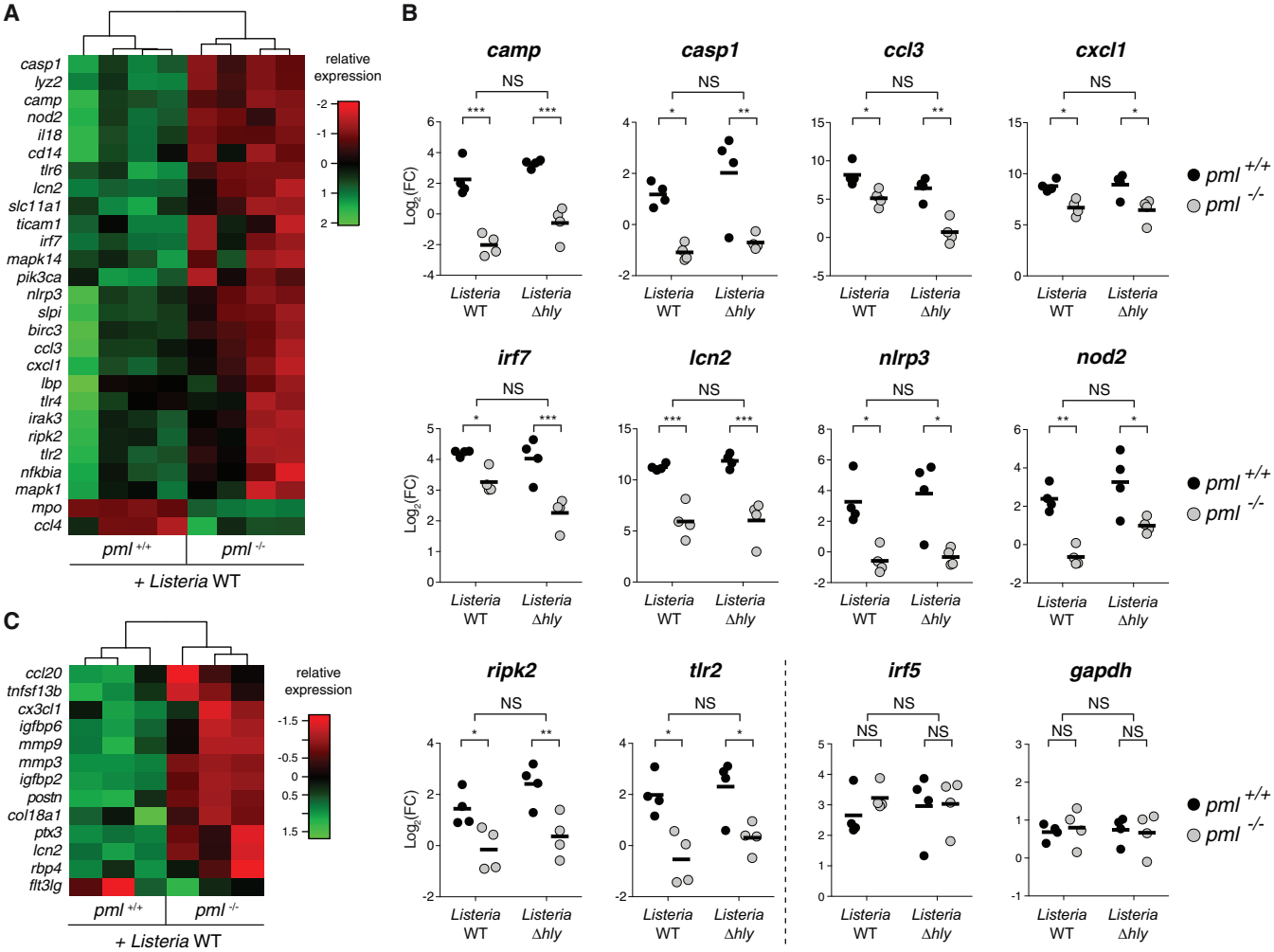

FIG 2 PML regulates gene expression and cytokine production. (A) Heat map of the 27 genes identified as significantly differentially regulated in $pml^{+/+}$ versus $pml^{-/-}$ MEFs after 24 h of infection with wild-type *Listeria* (Benjamini and Hochberg method, adjusted *P* value of <0.05; data from 4 independent experiments). Color code indicates relative expression compared with the expression in uninfected MEFs. (B) Expression levels of 10 representative genes differentially regulated in $pml^{+/+}$ versus $pml^{-/-}$ MEFs after infection with either wild-type or Δ*hly* *Listeria*. Data represent fold changes (FC) of gene expression levels in infected compared to uninfected MEFs (bars show mean results from 4 independent experiments; *, $P < 0.05$; **, $P < 0.01$; ***, $P < 0.001$; NS, not significant). *irf5* and *gapdh* are shown as examples of genes not regulated by PML. (C) Heat map of the 13 cytokines identified as significantly differentially secreted by $pml^{+/+}$ versus $pml^{-/-}$ MEFs after 24 h of infection with wild-type *Listeria* (Benjamini and Hochberg method, adjusted *P* value of <0.05; data from 3 independent experiments). Color code indicates relative expression compared with the expression in uninfected MEFs.

Listeria infection was differentially expressed after LLO treatment (see Table S3). This confirms our results showing that PML-dependent genes modulated in response to *Listeria* infection are independent of LLO.

In conclusion, our transcriptomic and proteomic screens identified a network of genes induced upon infection in a PML-dependent manner and highlighted a first role of PML in antibacterial responses, acting as a master regulator of genes involved in immunity against *Listeria*.

PML restricts *Listeria* replication in an LLO-dependent manner. To get further insights into how PML may restrict *Listeria*'s intracellular replication, we compared the replication efficiencies of wild-type and Δ*hly* *Listeria* in $pml^{+/+}$ or $pml^{-/-}$ MEFs. We took advantage of the observation that in our MEFs, and in contrast to other murine cell lines (41), a fraction of Δ*hly* bacteria can escape from the internalization vacuole and replicate intracellularly (Fig. 3; see also Fig. S2 in the supplemental material). MEFs were infected with *Listeria* and the numbers of intracellular bacteria were quantified after 1.5 h and 24 h of infection. Strikingly, we observed that, in contrast to the parental wild-type *Listeria* strain, the replication efficiencies of the Δ*hly* mutant were similar in

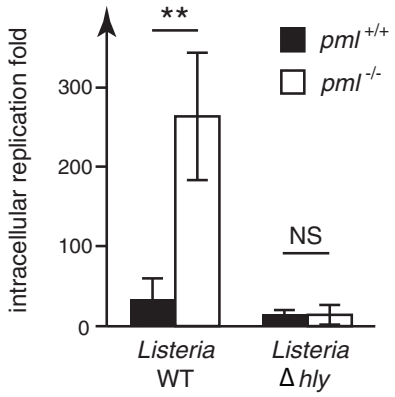

FIG 3 PML impairs replication of LLO-producing *Listeria*. $pml^{+/+}$ and $pml^{-/-}$ MEFs were infected with wild-type and Δ*hly Listeria* strains. The fold changes in intracellular replication were determined by calculating the ratio of intracellular bacteria at 24 h versus 1.5 h of infection (mean results ± standard deviations [SD] from 3 independent experiments; **, $P < 0.01$; NS, not significant; unpaired two-tailed Student's *t* test).

$pml^{+/+}$ and $pml^{-/-}$ MEFs (Fig. 3). This result demonstrates that PML restricts only LLO-producing bacteria and suggests that LLO exposure triggers, via PML, a host response against *Listeria*.

As the results for the PML-regulated genes and cytokines identified above were similar in cells infected with wild-type and Δ*hly Listeria*, we hypothesized that PML restricts LLO-producing bacteria by an additional, LLO-triggered pathway.

LLO triggers PML de-SUMOylation. In order to explore the link between LLO-producing *Listeria* and PML, we assessed whether infection leads to a modification of PML SUMOylation. We had previously demonstrated that pore formation in the host plasma membrane by the *Listeria* toxin LLO triggers de-SUMOylation of several host proteins during infection (20, 21). We treated CHO (Chinese hamster ovary) cells stably expressing a His_6-tagged version of the human PML protein (isoform III [PML-III]) with sublytic concentrations of purified LLO (from 0.3 to 3 nM). As a control, we treated CHO-PML cells in parallel with arsenic trioxide (As_2O_3), a drug successfully used to treat APL, which promotes PML multimerization and SUMOylation through Ubc9 recruitment to PML NBs (9, 30, 42, 43; reviewed in reference 44). Using immunoblot analysis of whole-cell extracts, we showed that, in sharp contrast to the effect of As_2O_3, which rapidly increases PML SUMOylation, LLO triggers a dose-dependent decrease in the level of PML high-molecular-weight species, corresponding to the well-described SUMOylated forms of PML (Fig. 4A and B). Of note, the total level of PML protein is not affected by LLO, pointing to de-SUMOylation events rather than degradation of PML, which is likely caused by the concomitant LLO-mediated degradation of Ubc9 (Fig. 4A and B). PML is thus a target of LLO-triggered loss of SUMOylation.

We further assessed that the effect of LLO on PML SUMOylation is pore dependent by using an LLO mutant (with a W-to-A change at position 492 [LLO^{W492A}]) that is able to bind cellular membranes but unable to form pores (20). This mutant did not affect PML SUMOylation or the Ubc9 level, in line with our previous findings that de-SUMOylation events mediated by LLO are pore dependent (Fig. 4B).

To confirm the effect of LLO on PML SUMOylation, we pulled down His_6-tagged PML proteins from CHO-PML cells treated with LLO or As_2O_3. Immunoblot analysis of the pulled-down PML reveals an increase in the intensity of PML SUMOylated forms after As_2O_3 treatment, whereas LLO decreases PML SUMOylation, particularly by the SUMO2/3 paralog (Fig. 4C). LLO can induce the degradation of some host SUMOylated proteins (20). To rule out a possible proteasome-dependent degradation of PML SUMOylated forms in response to LLO, we pretreated cells with the proteasome inhibitor MG132 and showed that this treatment does not block the LLO-induced decrease in PML SUMOylated forms (see Fig. S3 in the supplemental material). To-

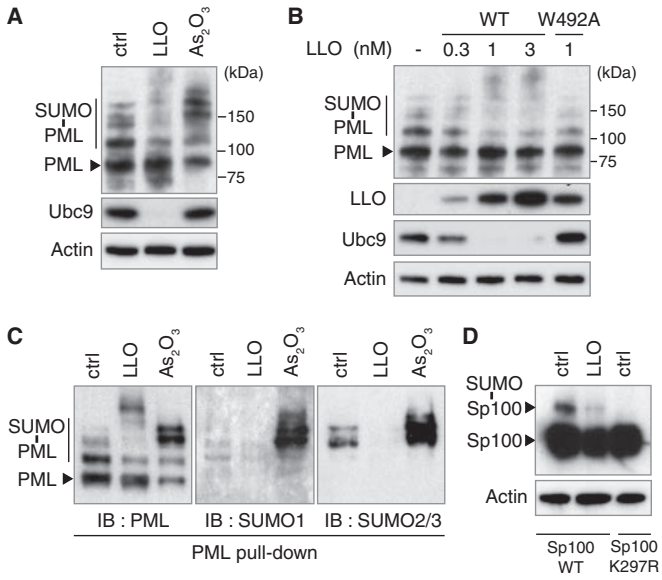

FIG 4 LLO induces PML and Sp100 de-SUMOylation. (A and B) Immunoblot analysis, using anti-PML, anti-Ubc9, anti-actin, and anti-LLO antibodies, of whole-cell lysates from CHO-PML cells treated with 1 nM LLO for 20 min or 10 μM As_2O_3 for 1 h (A) or treated for 20 min with either increasing doses of WT LLO or the non-pore-forming LLO^{W492A} mutant (B). (C) Immunoblot analysis, using anti-PML, anti-SUMO1 and anti-SUMO2/3 antibodies, of PML proteins from CHO-PML cells treated with 1 nM LLO for 20 min or with 10 μM As_2O_3 for 1 h; the PML proteins were pulled down by means of His_6 tags. (D) Immunoblot analysis, using anti-Sp100 and anti-actin antibodies, of whole-cell lysates from HeLa cells transfected with expression vectors for wild-type Sp100 or a non-SUMOylatable $Sp100^{K297R}$ mutant and treated with 3 nM LLO for 30 min. All immunoblots displayed were done under reducing conditions (+DTT).

gether, our data show that the plasma membrane pores formed by LLO lead to PML de-SUMOylation but not degradation. This is in sharp contrast to the effect of As_2O_3, which triggers PML hyper-SUMOylation, followed by PML polyubiquitylation and proteasomal degradation (30, 34, 35).

We finally monitored whether LLO also affects the SUMOylation level of Sp100, a constitutive structural component of PML NBs (45). HeLa cells transfected with expression vectors for wild-type Sp100 or a non-SUMOylatable $Sp100^{K297R}$ mutant were treated with LLO. Immunoblot analysis of whole-cell lysates shows a strong decrease in the level of the SUMO-modified form of Sp100 in response to LLO, indicating that this toxin triggers de-SUMOylation of not only PML but also other essential PML NB components (Fig. 4D).

LLO triggers PML multimerization. Short treatments with oxidative agents like As_2O_3 promote PML NB formation by inducing PML multimerization and association with the nuclear matrix, a nuclear fraction characterized by its insolubility and resistance to high salt and nuclease extractions (9, 11, 27, 30, 43, 46). LLO, like other pore-forming toxins (47), rapidly induces the production of reactive oxygen species (ROS) in the host cell (Fig. 5). We thus tested whether LLO would trigger PML multimerization. We performed immunoblot analysis of whole-cell lysates obtained under nonreducing conditions from LLO-treated CHO-PML cells. We observed PML multimers (with molecular masses above 200 kDa) that were not detected either under reducing conditions (Fig. 5A and Fig. 4) or when cells were pretreated with *N*-ethylmaleimide (NEM), an alkylating reagent that blocks free thiols (Fig. 5B). Altogether, these results strongly suggest that LLO induces an oxidative stress that leads to PML multimerization via intermolecular disulfide bonds, as observed for As_2O_3 (9, 11).

To decipher whether LLO triggers an association of PML with the nuclear matrix similarly to As_2O_3, we performed *in situ* high-salt extraction and DNase/RNase treatments to isolate nuclear matrices from LLO- or As_2O_3-treated CHO-PML cells. We observed that LLO-induced PML multimers were strongly associated with the nuclear

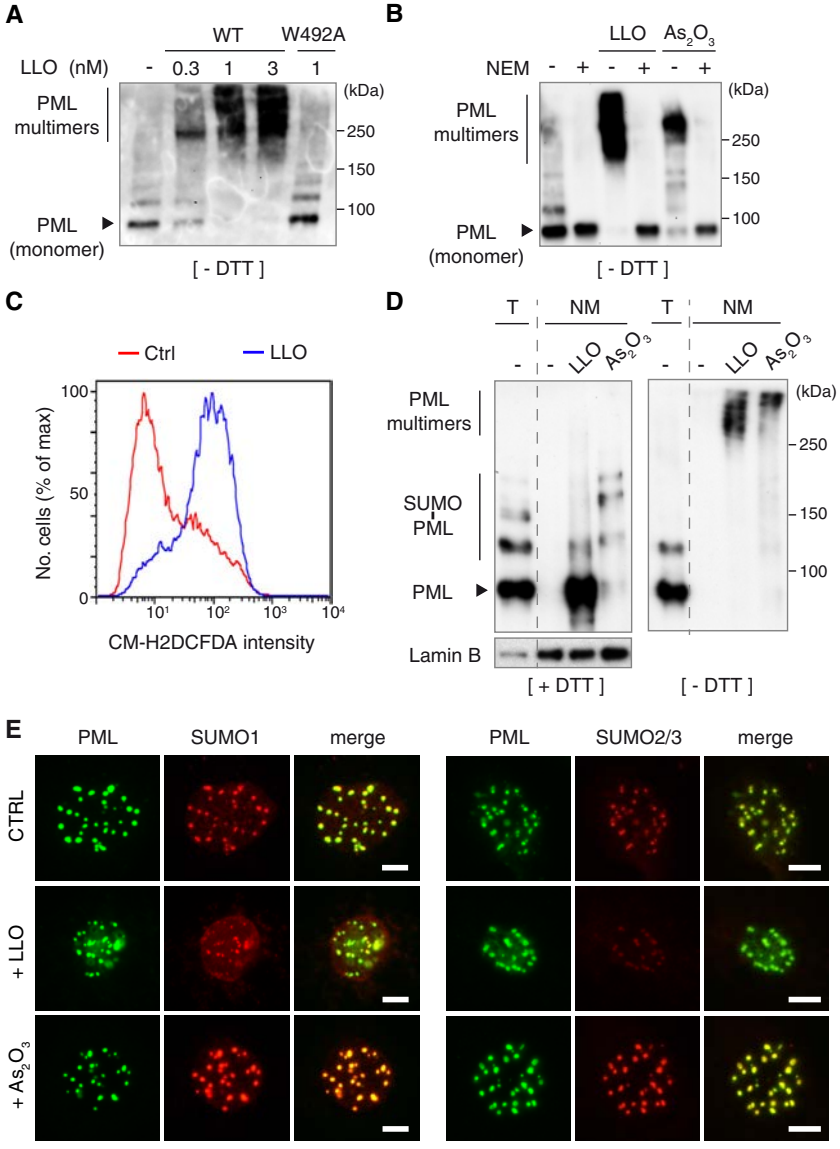

FIG 5 LLO induces PML multimerization and association with the nuclear matrix. (A and B) Immunoblot analysis under nonreducing conditions (without DTT [-DTT]), using anti-PML antibodies, of whole-cell lysates from CHO-PML cells. Cells were treated for 20 min with different doses of wild-type LLO or with LLO^{W492A} mutant (A) or pretreated with 100 μM NEM for 1 h and then treated with 1 nM LLO for 20 min or with 10 μM As_2O_3 for 1 h (B). (C) Representative results of flow cytometry analysis of CHO cells labeled with the ROS-sensitive CM-H_2DCFDA probe after incubation with 0.3 nM LLO for 2 min. (D) Immunoblot analysis under reducing (+DTT) or nonreducing (-DTT) conditions, using anti-PML and anti-lamin B antibodies, of total cell lysates (T) or nuclear matrix preparations (NM) from CHO-PML cells treated with 1 nM LLO for 20 min or 10 μM As_2O_3 for 1 h. (E) Immunofluorescence analysis, using anti-PML, anti-SUMO1, and anti-SUMO2/3 antibodies, of nuclear matrices from CHO-PML cells treated with 1 nM LLO for 20 min or 10 μM As_2O_3 for 1 h. Scale bar, 5 μm.

matrix (Fig. 5D). Interestingly, the predominant forms of nuclear matrix-associated PML are highly SUMOylated in As_2O_3-treated cells, as previously observed (9), but are poorly SUMOylated in LLO-treated cells (Fig. 5D). Finally, we performed immunofluorescence analysis of nuclear matrices obtained from CHO-PML cells treated with LLO or As_2O_3. Staining with anti-PML antibodies showed that LLO does not disrupt PML NBs (Fig. 5E). Staining with anti-SUMO1 and anti-SUMO2/3 antibodies revealed that LLO induces decreases of both SUMO1 and SUMO2/3 labeling of nuclear matrix-associated-PML, in sharp contrast to As_2O_3, which increases SUMO1 and SUMO2/3 labeling of these structures (Fig. 5E; see also Fig. S4 in the supplemental material).

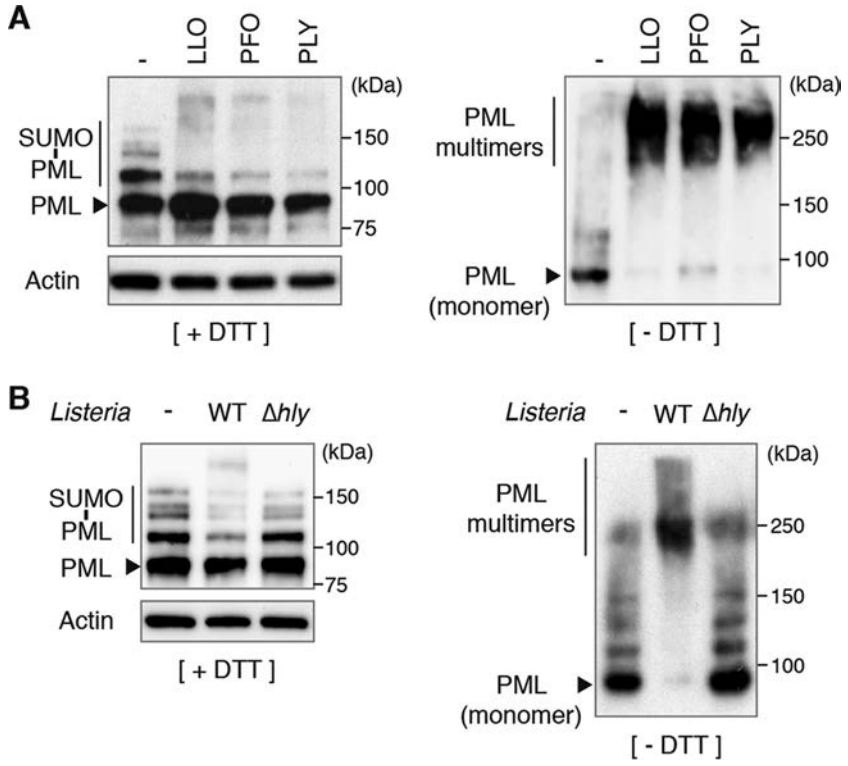

FIG 6 PML multimerizes and is de-SUMOylated in response to different pore-forming toxins and to *Listeria* infection. (A and B) Immunoblot analysis under reducing (+DTT) or nonreducing (-DTT) conditions, using anti-PML and anti-actin antibodies, of whole-cell lysates from CHO-PML cells treated for 20 min with different pore-forming toxins (A) or infected for 5 h with wild-type or Δ*hly Listeria* (B).

Taken together, our results show that exposure of host cells to LLO induces a covalent multimerization of PML proteins and their association with the nuclear matrix. However, in contrast to As_2O_3, exposure to LLO leads to a strong decrease in PML SUMOylation, consistent with the loss, rather than NB recruitment, of Ubc9.

Other bacterial pore-forming toxins trigger PML de-SUMOylation and multimerization. The degradation of Ubc9 and de-SUMOylation of host proteins can be triggered by other bacterial pore-forming toxins belonging, like LLO, to the family of cholesterol-dependent cytolysins (20, 48). We thus treated CHO-PML cells with two of these toxins, perfringolysin O (PFO; from *Clostridium perfringens*) and pneumolysin (PLY; from *Streptococcus pneumoniae*), and showed that these pore-forming toxins also lead to PML de-SUMOylation and multimerization (Fig. 6A). Thus, PML modifications may occur in response to different bacteria that produce pore-forming toxins.

Infection by *Listeria* affects PML SUMOylation and multimerization. In order to assess whether the PML modifications observed in response to purified LLO are also induced in the context of bacterial infection, we infected CHO-PML cells with wild-type or Δ*hly Listeria*. Cells were lysed after 5 h of infection and analyzed by immunoblotting experiments. We observed that infection with wild-type *L. monocytogenes* induces a strong multimerization of PML, associated with its global de-SUMOylation (Fig. 6B). Modifications of PML were not observed during infection with the Δ*hly Listeria* mutant (Fig. 6B). These results demonstrate that *Listeria* infection triggers PML multimerization and de-SUMOylation in an LLO-dependent manner.

LLO-induced PML de-SUMOylation impairs *Listeria*'s intracellular replication. Our results suggest that LLO-induced PML de-SUMOylation may trigger host antibacterial responses, impairing bacterial replication. To directly explore the role of PML de-SUMOylation in *Listeria*'s intracellular replication, we transfected HeLa cells with a vector expressing a truncated form of the iE1 protein from human cytomegalovirus

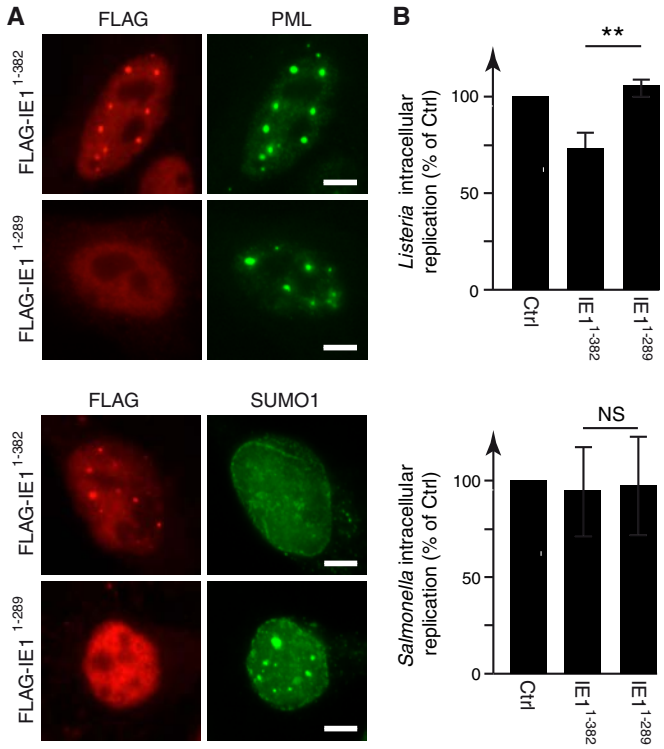

FIG 7 Induction of PML de-SUMOylation impairs *Listeria*'s intracellular replication. (A) Immunofluorescence analysis of nuclei from HeLa cells transfected with expression vectors for FLAG-iE1$^{1-382}$ or FLAG-iE1$^{1-289}$ and stained with anti-FLAG, anti-PML, and anti-SUMO1 antibodies. Scale bar, 5 μm. (B) HeLa cells transfected with FLAG-iE1$^{1-382}$ or FLAG-iE1$^{1-289}$ were infected with *Listeria* or *Salmonella*. Fold changes in intracellular replication were calculated as the ratio of intracellular bacteria at 24 h versus 1.5 h of infection and are expressed as percentages of the result for the control (mean results $\pm$ SD from 3 to 4 independent experiments; **, $P < 0.01$; NS, not significant; unpaired two-tailed Student's *t* test).

(including residues 1 to 382 [iE1$^{1-382}$]). This protein induces PML de-SUMOylation without disrupting PML NBs, although other effects on PML cannot be formally excluded (Fig. 7A; see also Fig. S5 in the supplemental material) (49). We used as controls cells transfected with an empty vector or with an expression vector for a shorter iE1 protein (iE1$^{1-289}$) that does not trigger PML de-SUMOylation (Fig. 7A; see also Fig. S5). HeLa cells transfected with these different plasmids were then infected by *Listeria*, and the numbers of intracellular bacteria were quantified 1.5 h and 24 h after infection (Fig. 7B). Strikingly, we observed a consistent decrease in the replication efficiency of bacteria in cells transfected with iE1$^{1-382}$ compared to the bacterial replication in cells transfected with an empty vector or with iE1$^{1-289}$ (Fig. 7B). In contrast, when the same experiment was performed with *Salmonella*, similar intracellular replication efficiencies were observed under all test conditions, indicating that PML SUMOylation does not restrict this bacterium, in agreement with our previous *in vivo* and *in vitro* data (Fig. 1B and C and 7B). Taken together, these data establish that PML de-SUMOylation impairs *Listeria* infection in the host cell, thereby supporting our hypothesis that LLO-induced PML SUMO deconjugation is a contributor to bacterial replication dampening.

DISCUSSION

In this study, we analyzed the role of PML and its SUMOylation in bacterial infection. By studying MEFs' responses to *Listeria* infection, we characterized a network of genes and cytokines that are involved in innate immunity and regulated by PML. The lack of induction of these genes in *pml*$^{-/-}$ cells may explain, albeit partially, the increased sensitivity of these mice to *Listeria* infection. Of note, we established that the expression of these genes does not depend on the presence of LLO (Fig. 8). Previous studies have

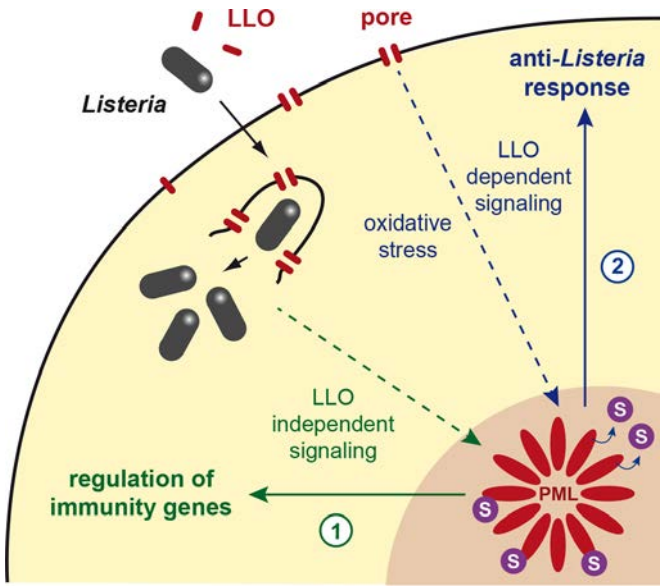

FIG 8 Model illustrating the roles of PML and its SUMOylation in anti-*Listeria* responses. (1) Infection with *Listeria* triggers the expression of genes involved in innate immunity. A fraction of these genes are regulated by PML, in an LLO-independent manner. (2) Pore formation in the host plasma membranes by LLO induces Ubc9 degradation and oxidative stress, leading to PML de-SUMOylation, multimerization, and association with the nuclear matrix. We propose that this state of PML is sensed as a danger signal by the cell, which triggers in response the dampening of bacterial replication.

established that PML regulates either positively or negatively the expression of genes involved in antiviral responses and, more particularly, of interferon (IFN)-stimulated genes (ISGs) (50–55). Here, in the context of *Listeria* infection, 17 of the 36 PML-regulated genes and cytokines identified are actually known IFN-inducible genes (based on the Interferome database, version 2.01 [56]). This suggests that some of the mechanisms involved in the PML regulation of ISGs in the context of viral infection might be shared during infection by a bacterial pathogen, such as *Listeria*. Besides IFN-inducible genes, PML was also shown to regulate NF-kB-dependent genes, such as interleukin-6 (IL-6) (37, 53). Here, in the context of *Listeria* infection, we do not observe a significant difference between $pml^{+/+}$ and $pml^{-/-}$ MEFs in their expression of *il6* or other established NF-kB-dependent genes, such as *tnf-α* (encoding tumor necrosis factor alpha), *ccl5*, *il1b* (encoding interleukin-1b), *il12a*, *il12b*, and *trl9* (see Tables S1 and S2 in the supplemental material). This suggests that PML does not regulate NF-kB genes in the context of *Listeria* infection.

In addition to this role of PML in the regulation of immunity genes, we demonstrate that, in MEFs, PML restricts specifically the replication of LLO-expressing *Listeria* but not that of a Δ*hly* mutant. As PML-dependent genes were similarly regulated in cells infected with wild-type and Δ*hly Listeria*, we conclude that PML restricts *Listeria* by an additional, LLO-dependent mechanism, relying, at least in part, on PML de-SUMOylation (Fig. 8). This echoes the intrinsic antiviral activities of PML in the context of viral infections. PML NBs can, for example, mediate the epigenetic silencing of viral genomes, entrap newly assembled viral capsids, or interfere with early viral events after relocalization in the cytoplasm (reviewed in reference 55). In the case of *Listeria* infection, we demonstrated that host plasma membrane perforation by LLO triggers PML oxidation, multimerization, and association with the nuclear matrix, in striking similarity to the results of arsenic trioxide exposure. However, in contrast to As_2O_3-treated cells, where Ubc9 recruitment into NBs yields a massive PML hyper-SUMOylation (9, 11), PML NBs are paradoxically de-SUMOylated in LLO-treated cells, because of concomitant Ubc9 degradation and, possibly, also recruitment of SUMO proteases. These events generate an unprecedented situation compared to several viral

infections that induce PML degradation and/or PML NB disruption to counteract PML antiviral activity (16, 17).

Strikingly, we observed that PML does not control infection by *Salmonella* Typhimurium, even though this pathogen was also shown to induce a decrease in the Ubc9 level (25). Further characterization of the putative PML-regulated genes induced during *Salmonella* infection or the effect of *Salmonella* on PML SUMOylation/multimerization will be required to fully understand the differences in PML-dependent sensitivity between *Listeria* and *Salmonella*. Interestingly, *Shigella flexneri*, in addition to its effect on the Ubc9 level, was shown to induce a two-fold increase in the number of PML NBs in HeLa cells, which was not observed during incubation with a non-invasive avirulent strain (22). The putative role of PML in *Shigella* infection, however, remains unknown.

In conclusion, *Listeria* LLO defines a novel means, i.e., PML de-SUMOylation, through which pathogens unexpectedly activate PML-enforced restriction of their replication. We propose that PML acts as a sensor for bacteria that produce pore-forming toxins, illustrating the concept, initially proposed for viruses but now extended to bacteria, that intranuclear bodies play critical roles in responses against invading pathogens.

We previously demonstrated that the global de-SUMOylation triggered by LLO is actually beneficial for *Listeria* infection (20). The case of PML, whose de-SUMOylation counteracts bacterial infection, illustrates how SUMO alterations of some host proteins can also constitute danger signals for the cells, leading to a response aimed to limit infection. Our data thus highlight the fine balance between toxin-induced alterations of host cell functions that are beneficial for infection and toxin damages sensed by host cells leading to antibacterial responses.

MATERIALS AND METHODS

Plasmids. The cDNAs encoding hCMV iE1$^{1-328}$ and iE1$^{1-289}$ fused to an N-terminal FLAG tag were obtained by gene synthesis (Integrated DNA Technologies, Inc.) and then cloned into the pCDNA.3 vector (Invitrogen) (pCDNA3-FLAG-hCMV iE1$^{1-382}$ [BUG 3779; Bacteria-Cell Interactions laboratory's bacteria collection] and pCDNA3-FLAG-hCMV iE1$^{1-289}$ [BUG 3780]). The plasmids encoding YFP-CBD, a yellow fluorescent protein (YFP) chimera protein of the cell wall binding domain (CBD) from the *Listeria* phage endolysin Ply118 (BUG 2305; kind gift from J. Swanson, University of Michigan Medical School, Ann Arbor, MI, USA), and Sp100 (pSG5-Sp100^{WT} [BUG 4134] and its derivative pSG5-Sp100^{K297R} [BUG 4135]) have been described previously (11, 57).

Cell culture and transfections. Mouse embryo fibroblasts (MEFs) derived from *pml*$^{+/+}$ or *pml*$^{-/-}$ mice and immortalized with a plasmid expressing simian virus 40 (SV40) large T antigen and CHO cells stably expressing His_6-tagged human PML isoform III (CHO-PML) have been described previously (30). These cells were cultivated in Dulbecco modified Eagle medium (DMEM)-GlutaMAX (Invitrogen) supplemented with 10% fetal calf serum (FCS). CHO-PML cells were additionally cultivated with 1 mg/ml hygromycin B (Invitrogen) to maintain the expression of the human PML isoform III (PML-III). HeLa cells (CCL-2 from ATCC [American Type Culture Collection]) were cultivated in minimal essential medium (MEM)-GlutaMAX (Invitrogen) supplemented with 10% FCS, MEM nonessential amino acids (Invitrogen), and 1 mM sodium pyruvate (Invitrogen).

For transfections, HeLa cells and MEFs were seeded at a density of 1.25×10^5 cells per 400-mm^2 well. The next day, cells were transfected with 1.5 μg of DNA using Lipofectamine LTX reagents (Invitrogen) for 24 h.

Bacterial strains. The strains used in this study were *Listeria monocytogenes* strain EGD (BUG 600), an *L. monocytogenes* EGD Δ*hly* mutant (BUG 3650 [58]), *L. monocytogenes* EGDe.PrfA* (BUG 3057), and *Salmonella* Typhimurium strain SR-11 (BUG 3044; kind gift of F. Norel and V. Robbe-Saule, Institut Pasteur, Paris, France). *Listeria* strains were grown in brain heart infusion (BHI) broth or agar plates (BD Difco), whereas *Salmonella* Typhimurium was grown in Luria-Bertani (LB) broth or agar plates (BD Difco).

Bacterial infections. For *in vivo* infection, procedures were performed in accordance with protocols approved by the Animal Experimentation Ethics Committee of the Institut Pasteur (permit number 03-49), applying the guidelines of the European Commission for the handling of laboratory animals, Directive 2010/63/EU. The protocols were approved by the veterinary staff of the Institut Pasteur animal facility and were performed in compliance with NIH Animal Welfare Assurance number A5476-1, issued on 31 July 2012. Amounts of 5×10^5 *Listeria* or 1×10^5 *Salmonella* bacteria were injected intravenously into *pml*$^{+/+}$ or *pml*$^{-/-}$ mice (described in reference 59), and the CFUs per organ were enumerated at 72 h postinfection.

For *in vitro* infections, MEFs and CHO-PML cells were seeded, respectively, at a density of 2.5×10^5 or 1.25×10^5 cells per 400-mm^2 well the day before infection. For transfected HeLa cells, infections were performed 24 h after transfection. Bacteria were cultured overnight, subcultured 1:20 in BHI or LB medium at 37°C until reaching an optical density at 600 nm (OD_{600}) of 1.0 for *Listeria* or 1.5 for *Salmonella*, and washed twice in phosphate-buffered saline (PBS). MEFs or CHO-PML or HeLa cells were serum starved for 1 h before the addition of bacteria. Bacteria were added to cells at a multiplicity of infection

(MOI) of 50 for *Listeria* or 2 for *Salmonella*. After 1 h of infection, cells were washed and incubated with fresh medium supplemented with 10% FCS and 50 μg/ml gentamicin (Euromedex) to kill extracellular bacteria. For immunoblot analysis, infected cells were lysed 5 h after the beginning of infection with Laemmli buffer (0.125 M Tris, pH 6.8, 4% SDS, 20% glycerol, 100 mM dithiothreitol [DTT], 0.0025% bromophenol blue). To quantify intracellular bacteria, infected cells were lysed 1.5, 5, or 24 h after the beginning of infection with PBS–0.2% Triton X-100 (Sigma), and the number of viable intracellular bacteria released from the cells was assessed by plating on BHI or LB agar plates as previously described (60).

Analysis of gene expression from infected cells. RNAs from MEFs infected or not for 24 h with wild-type or Δ*hly Listeria* (EGD strain) were extracted using miRNeasy minikits (Qiagen). Four hundred nanograms of RNA was reverse transcribed using RT^2 first strand kits (Qiagen). Real-time PCRs were then performed using a CFX384 real-time PCR detection system (Bio-Rad), RT^2 SYBR green master mix, and RT^2 Profiler mouse antibacterial PCR arrays (Qiagen). Gene expression was then normalized using the expression levels of 5 reference genes (*actb*, *b2m*, *gapdh*, *gusb*, and *hsp90a1*).

Analysis of cytokine secretion from infected cells. Five hundred microliters of supernatants from MEFs infected or not for 24 h with wild-type or Δ*hly Listeria* (EGD strain) were collected, centrifuged for 10 min at 13,000 $\times$ *g* to remove cell remnants, and used to probe Proteome Profiler mouse XL cytokine arrays (R&D Systems), following the manufacturer's instructions. Cytokine levels were quantified using the G:Box gel documentation system and the associated GeneTools software (Syngene).

Statistical analysis of gene expression and cytokine secretion. Both gene expression and cytokine secretion data were analyzed using R version 3.3.0 (61) and the limma Bioconductor package version 3.28.2 (62). The replicate effect was included in the linear models as a blocking factor alongside the variables of interest. Raw *P* values were adjusted for multiple testing according to the Benjamini and Hochberg (BH) procedure (63), and features with an adjusted *P* value lower than 0.05 were considered differentially expressed.

Pore-forming toxins and arsenic treatment. For treatments with pore-forming toxins or arsenic trioxide (As_2O_3, single-element standard solution, 1,000 mg/liter stock solution; Sigma-Aldrich), MEFs and CHO-PML cells were seeded, respectively, at a density of 2.5 $\times$ 10^5 or 1.25 $\times$ 10^5 cells per 400-mm^2 well the day before treatment. For His pulldown of His_6-tagged PML, CHO-PML cells were seeded at a density of 2.5 $\times$ 10^6 cells in 75-cm^2 flasks the day before treatment. Cells were serum starved for 2 h before treatment.

Wild-type LLO (LLO^{WT}) and LLO^{W492A} proteins were purified as previously described (64). Purified PFO and PLY were kindly provided by T. Mitchell (University of Glasgow, Glasgow, Scotland, UK). Purified pore-forming toxins were added directly to the culture medium as indicated in the text. PFO and PLY were used at the same hemolytic titre as LLO.

Arsenic trioxide was added to the culture medium at a final concentration of 10 μM for 1 h. For proteasome inhibition, CHO-PML cells were pretreated with 10 μM MG132 (Z-Leu-Leu-Leu-al; Sigma-Aldrich) or dimethyl sulfoxide (DMSO) for 5 h, washed, and then incubated with LLO or As_2O_3. *N*-Ethyl-maleimide (NEM; Sigma-Aldrich) was added to the culture medium for 1 h, and cells were then washed and incubated with LLO or As_2O_3. After treatment, cells were lysed directly in Laemmli buffer. For analysis under nonreducing conditions, cells were lysed in Laemmli buffer without DTT.

His pulldown assays. His_6-tagged PML was isolated from CHO-PML cells lysed with lysis buffer (6 M guanidium HCl, 10 mM Tris, 100 mM sodium phosphate buffer [pH 8.0], 5 mM β-mercaptoethanol, 1 mM imidazole). The cell lysates were sonicated and centrifuged for 15 min at 16,000 $\times$ *g*, and the corresponding supernatants were incubated overnight at 4°C with 250 μl of packed Ni-nitrilotriacetic acid (NTA) agarose beads (Qiagen) prewashed in lysis buffer. After incubation, the beads were washed once in lysis buffer, once in wash buffer, pH 8.0 (8 M urea, 10 mM Tris, 100 mM sodium phosphate buffer [pH 8.0], 0.1% Triton X-100, 5 mM β-mercaptoethanol), and three times in wash buffer, pH 6.3 (8 M urea, 10 mM Tris, 100 mM sodium phosphate buffer [pH 6.3], 0.1% Triton X-100, 5 mM β-mercaptoethanol, 10 mM imidazole). His_6-tagged PML proteins were then eluted from the beads using elution buffer (200 mM imidazole, 5% SDS, 150 mM Tris-HCl [pH 6.7], 30% glycerol, 720 mM β-mercaptoethanol, 0.0025% bromophenol blue).

Flow cytometry analysis. CHO cells were treated with 0.3 nM LLO for 2 min, washed, and then labeled with 1 μM CM-H_2DCFDA (chloromethyl derivative of 2′,7′-dichlorodihydrofluorescein diacetate; Life Technologies, Inc.) for 20 min. Cells were then detached using Versene solution and analyzed with a FACSCalibur flow cytometer (Becton, Dickinson).

***In situ* nuclear matrix preparation.** Nuclear matrices were prepared as described previously (11). CHO-PML cells were seeded at a density of 3 $\times$ 10^5 cells on 10-cm^2 coverslips or 2.5 $\times$ 10^6 cells in 80-cm^2 plates the day before treatment. After LLO or As_2O_3 treatment, cells were fixed for 15 min at 4°C in Kern matrix buffer (KMB) (10 mM MES [morpholineethanesulfonic acid], pH 6.2, 10 mM NaCl, 1.5 mM $MgCl_2$, protease inhibitors [complete protease inhibitor cocktail tablets; Roche], 10% glycerol) and then washed twice with KMB containing 1% NP-40. After three additional washes with KMB, cells were incubated with 50 μg/ml RNase A and 0.3 U/ml micrococcal nuclease for 30 min at 25°C. Cells were then washed three times with KMB containing 2 M NaCl for 15 min at 4°C and three times with KMB. Nuclear matrices were then resuspended in Laemmli buffer for immunoblot analysis or fixed in PBS–4% paraformaldehyde (PFA) for 10 min, followed by 100% methanol for 5 min, for immunofluorescence analysis.

Western blot analysis. Cells lysed in Laemmli buffer, proteins eluted from His pulldown assays, and nuclear matrix preparations were resolved by SDS-polyacrylamide gel electrophoresis. Proteins were then transferred to polyvinylidene difluoride (PVDF) membranes and detected after incubation with specific antibodies with Pierce enhanced chemiluminescence (ECL) 2 Western blotting substrate (Fisher

Scientific). The primary antibodies used for immunoblot analysis are described in Table S4 in the supplemental material. Rabbit polyclonal antibodies against LLO (R176), SUMO1 (R204), and SUMO3 (R205 and R206) were obtained in-house by immunizing rabbits with recombinant proteins produced in *Escherichia coli*, followed by affinity purification of the immune serum. Antibodies against human PML were obtained in-house from chicken eggs immunized with glutathione *S*-transferase (GST)–PML-III fusion protein produced in *Escherichia coli* (34). Antibodies against human Sp100A were obtained in-house by immunizing rabbits with recombinant full-length hSp100A (11). Anti-mouse and anti-rabbit horseradish peroxidase (HRP)-conjugated antibodies (AbCys) were used as secondary antibodies. All immunoblots displayed in the figures are representative of at least two independent experiments.

Immunofluorescence analysis. Cells on coverslips were incubated after methanol fixation with primary and then secondary antibodies in PBS–1% BSA, and mounted in Fluoromount (Interchim). The antibodies used for immunofluorescence analysis are described in Table S4 in the supplemental material. Mouse monoclonal antibody against human PML (2′C7) was obtained from murine hybridoma in-house using purified PML-III–MBP fusion protein. Alexa Fluor 488- or 546-labeled anti-mouse and anti-rabbit antibodies (Molecular Probes), Texas red-labeled anti-goat antibodies, and fluorescein isothiocyanate (FITC)-conjugated anti-mouse antibodies (Jackson Immunology) were used as secondary antibodies. All images displayed in the figures are representative fields from at least two independent experiments.

SUPPLEMENTAL MATERIAL

Supplemental material for this article may be found at https://doi.org/10.1128/mBio.02179-16.

FIG S1, PDF file, 1.6 MB.
FIG S2, PDF file, 3.4 MB.
FIG S3, PDF file, 1.5 MB.
FIG S4, PDF file, 3.4 MB.
FIG S5, PDF file, 3.9 MB.
TABLE S1, XLSX file, 0.1 MB.
TABLE S2, XLSX file, 0.1 MB.
TABLE S3, XLSX file, 0.1 MB.
TABLE S4, PDF file, 0.1 MB.

ACKNOWLEDGMENTS

We thank E. Gouin for help with antibody production, P. P. Pandolfi for PML knockout mice, M. Pla and the animal house facility staff for their help with animal handling, F. Norel and V. Robbe-Saule for the *Salmonella* strain, J. Swanson for the YFP-CBD-encoding plasmid, and T. Mitchell for *Clostridium* and *Streptococcus* pore-forming toxins.

Work in P.C.'s laboratory received financial support from Institut Pasteur, INSERM, INRA, National Research Agency (ANR) (ERANET PathoGenomics LISTRESS ANR-10-PATH-001-01 and ERANET Infect-ERA PROANTILIS ANR-13-IFEC-0004-02), the French Government's Investissement d'Avenir program, Laboratoire d'Excellence "Integrative Biology of Emerging Infectious Diseases" (ANR-10-LABX-62-IBEID), the European Research Council (ERC) (advanced grant number 233348 MODELIST and H2020-ERC-2014-ADG 670823-BacCellEpi), the Fondation le Roch les Mousquetaires, the International Balzan Prize Fondation, and the Fondation Louis-Jeantet. Work in H.D.T.'s laboratory is supported by ANR Investissements d'Avenir program (ANR-11-PHUC-002, ANR-10-IHUB-0002), Association pour la Recherche contre le Cancer (Griffuel Award to H.D.T.), and ERC (STEMAPL advanced grant). D.R. is a research associate from INSERM, and P.C. is a senior international research scholar of the Howard Hughes Medical Institute.

The funders had no role in study design, data collection and interpretation, or the decision to submit the work for publication.

REFERENCES

1. de Thé H, Chomienne C, Lanotte M, Degos L, Dejean A. 1990. The t(15;17) translocation of acute promyelocytic leukaemia fuses the retinoic acid receptor alpha gene to a novel transcribed locus. Nature 347:558–561. https://doi.org/10.1038/347558a0.
2. de Thé H, Lavau C, Marchio A, Chomienne C, Degos L, Dejean A. 1991. The PML-RAR alpha fusion mRNA generated by the t(15;17) translocation in acute promyelocytic leukemia encodes a functionally altered RAR. Cell 66:675–684. https://doi.org/10.1016/0092-8674(91)90113-D.
3. Goddard AD, Borrow J, Freemont PS, Solomon E. 1991. Characterization of a zinc finger gene disrupted by the t(15;17) in acute promyelocytic leukemia. Science 254:1371–1374. https://doi.org/10.1126/science.1720570.
4. Kakizuka A, Miller WH, Jr, Umesono K, Warrell RP, Jr, Frankel SR, Murty VV, Dmitrovsky E, Evans RM. 1991. Chromosomal translocation t(15;17) in human acute promyelocytic leukemia fuses RAR alpha with a novel putative transcription factor, PML. Cell 66:663–674. https://doi.org/10.1016/0092-8674(91)90112-C.

5. Pandolfi PP, Grignani F, Alcalay M, Mencarelli A, Biondi A, LoCoco F, Grignani F, Pelicci PG. 1991. Structure and origin of the acute promyelocytic leukemia myl/RAR alpha cDNA and characterization of its retinoid-binding and transactivation properties. Oncogene 6:1285–1292.
6. Bernardi R, Pandolfi PP. 2007. Structure, dynamics and functions of promyelocytic leukaemia nuclear bodies. Nat Rev Mol Cell Biol 8:1006–1016. https://doi.org/10.1038/nrm2277.
7. Lallemand-Breitenbach V, de Thé H. 2010. PML nuclear bodies. Cold Spring Harb Perspect Biol 2:a000661. https://doi.org/10.1101/cshperspect.a000661.
8. Banani SF, Rice AM, Peeples WB, Lin Y, Jain S, Parker R, Rosen MK. 2016. Compositional control of phase-separated cellular bodies. Cell 166:651–663. https://doi.org/10.1016/j.cell.2016.06.010.
9. Jeanne M, Lallemand-Breitenbach V, Ferhi O, Koken M, Le Bras M, Duffort S, Peres L, Berthier C, Soilihi H, Raught B, de Thé H. 2010. PML/RARA oxidation and arsenic binding initiate the antileukemia response of As2O3. Cancer Cell 18:88–98. https://doi.org/10.1016/j.ccr.2010.06.003.
10. de Thé H, Chen Z. 2010. Acute promyelocytic leukaemia: novel insights into the mechanisms of cure. Nat Rev Cancer 10:775–783. https://doi.org/10.1038/nrc2943.
11. Sahin U, Ferhi O, Jeanne M, Benhenda S, Berthier C, Jollivet F, Niwa-Kawakita M, Faklaris O, Setterblad N, de Thé H, Lallemand-Breitenbach V. 2014. Oxidative stress-induced assembly of PML nuclear bodies controls sumoylation of partner proteins. J Cell Biol 204:931–945. https://doi.org/10.1083/jcb.201305148.
12. Tessier S, Martin-Martin N, de Thé H, Carracedo A, Lallemand-Breitenbach V. 2016. PML, a protein at the cross road of oxidative stress and metabolism. Antioxid Redox Signal https://doi.org/10.1089/ars.2016.6898.
13. Sahin U, Ferhi O, Carnec X, Zamborlini A, Peres L, Jollivet F, Vitaliano-Prunier A, de Thé H, Lallemand-Breitenbach V. 2014. Interferon controls SUMO availability via the Lin28 and let-7 axis to impede virus replication. Nat Commun 5:4187. https://doi.org/10.1038/ncomms5187.
14. Bernardi R, Papa A, Pandolfi PP. 2008. Regulation of apoptosis by PML and the PML-NBs. Oncogene 27:6299–6312. https://doi.org/10.1038/onc.2008.305.
15. Geoffroy MC, Hay RT. 2009. An additional role for SUMO in ubiquitin-mediated proteolysis. Nat Rev Mol Cell Biol 10:564–568. https://doi.org/10.1038/nrm2707.
16. Geoffroy MC, Chelbi-Alix MK. 2011. Role of promyelocytic leukemia protein in host antiviral defense. J Interferon Cytokine Res 31:145–158. https://doi.org/10.1089/jir.2010.0111.
17. Everett RD, Boutell C, Hale BG. 2013. Interplay between viruses and host sumoylation pathways. Nat Rev Microbiol 11:400–411. https://doi.org/10.1038/nrmicro3015.
18. Cossart P. 2011. Illuminating the landscape of host-pathogen interactions with the bacterium *Listeria monocytogenes*. Proc Natl Acad Sci U S A 108:19484–19491. https://doi.org/10.1073/pnas.1112371108.
19. Flotho A, Melchior F. 2013. Sumoylation: a regulatory protein modification in health and disease. Annu Rev Biochem 82:357–385. https://doi.org/10.1146/annurev-biochem-061909-093311.
20. Ribet D, Hamon M, Gouin E, Nahori MA, Impens F, Neyret-Kahn H, Gevaert K, Vandekerckhove J, Dejean A, Cossart P. 2010. *Listeria monocytogenes* impairs SUMOylation for efficient infection. Nature 464:1192–1195. https://doi.org/10.1038/nature08963.
21. Impens F, Radoshevich L, Cossart P, Ribet D. 2014. Mapping of SUMO sites and analysis of SUMOylation changes induced by external stimuli. Proc Natl Acad Sci U S A 111:12432–12437. https://doi.org/10.1073/pnas.1413825111.
22. Sidik SM, Salsman J, Dellaire G, Rohde JR. 2015. *Shigella* infection interferes with SUMOylation and increases PML-NB number. PLoS One 10:e0122585. https://doi.org/10.1371/journal.pone.0122585.
23. Fritah S, Lhocine N, Golebiowski F, Mounier J, Andrieux A, Jouvion G, Hay RT, Sansonetti P, Dejean A. 2014. Sumoylation controls host anti-bacterial response to the gut invasive pathogen *Shigella flexneri*. EMBO Rep 15:965–972. https://doi.org/10.15252/embr.201338386.
24. Verma S, Mohapatra G, Ahmad SM, Rana S, Jain S, Khalsa JK, Srikanth CV. 2015. *Salmonella* engages host microRNAs to modulate SUMOylation: a new arsenal for intracellular survival. Mol Cell Biol 35:2932–2946. https://doi.org/10.1128/MCB.00397-15.
25. Decque A, Joffre O, Magalhaes JG, Cossec JC, Blecher-Gonen R, Lapaquette P, Silvin A, Manel N, Joubert PE, Seeler JS, Albert ML, Amit I, Amigorena S, Dejean A. 2015. Sumoylation coordinates the repression of inflammatory and anti-viral gene-expression programs during innate sensing. Nat Immunol 17:140–149. https://doi.org/10.1038/ni.3342.
26. Kamitani T, Kito K, Nguyen HP, Wada H, Fukuda-Kamitani T, Yeh ET. 1998. Identification of three major sentrinization sites in PML. J Biol Chem 273:26675–26682. https://doi.org/10.1074/jbc.273.41.26675.
27. Müller S, Matunis MJ, Dejean A. 1998. Conjugation with the ubiquitin-related modifier SUMO-1 regulates the partitioning of PML within the nucleus. EMBO J 17:61–70. https://doi.org/10.1093/emboj/17.1.61.
28. Ishov AM, Sotnikov AG, Negorev D, Vladimirova OV, Neff N, Kamitani T, Yeh ET, Strauss JF, III, Maul GG. 1999. PML is critical for ND10 formation and recruits the PML-interacting protein daxx to this nuclear structure when modified by SUMO-1. J Cell Biol 147:221–234. https://doi.org/10.1083/jcb.147.2.221.
29. Zhong S, Müller S, Ronchetti S, Freemont PS, Dejean A, Pandolfi PP. 2000. Role of SUMO-1-modified PML in nuclear body formation. Blood 95:2748–2752.
30. Lallemand-Breitenbach V, Zhu J, Puvion F, Koken M, Honoré N, Doubeikovsky A, Duprez E, Pandolfi PP, Puvion E, Freemont P, de Thé H. 2001. Role of promyelocytic leukemia (PML) sumolation in nuclear body formation, 11S proteasome recruitment, and As2O3-induced PML or PML/retinoic acid receptor alpha degradation. J Exp Med 193:1361–1371. https://doi.org/10.1084/jem.193.12.1361.
31. Vertegaal AC, Andersen JS, Ogg SC, Hay RT, Mann M, Lamond AI. 2006. Distinct and overlapping sets of SUMO-1 and SUMO-2 target proteins revealed by quantitative proteomics. Mol Cell Proteomics 5:2298–2310. https://doi.org/10.1074/mcp.M600212-MCP200.
32. Cuchet-Lourenço D, Boutell C, Lukashchuk V, Grant K, Sykes A, Murray J, Orr A, Everett RD. 2011. SUMO pathway dependent recruitment of cellular repressors to herpes simplex virus type 1 genomes. PLoS Pathog 7:e1002123. https://doi.org/10.1371/journal.ppat.1002123.
33. Galisson F, Mahrouche L, Courcelles M, Bonneil E, Meloche S, Chelbi-Alix MK, Thibault P. 2011. A novel proteomics approach to identify SUMOylated proteins and their modification sites in human cells. Mol Cell Proteomics 10:M110.004796. https://doi.org/10.1074/mcp.M110.004796.
34. Lallemand-Breitenbach V, Jeanne M, Benhenda S, Nasr R, Lei M, Peres L, Zhou J, Zhu J, Raught B, de Thé H. 2008. Arsenic degrades PML or PML-RARalpha through a SUMO-triggered RNF4/ubiquitin-mediated pathway. Nat Cell Biol 10:547–555. https://doi.org/10.1038/ncb1717.
35. Tatham MH, Geoffroy MC, Shen L, Plechanovova A, Hattersley N, Jaffray EG, Palvimo JJ, Hay RT. 2008. RNF4 is a poly-SUMO-specific E3 ubiquitin ligase required for arsenic-induced PML degradation. Nat Cell Biol 10:538–546. https://doi.org/10.1038/ncb1716.
36. Ivanschitz L, Takahashi Y, Jollivet F, Ayrault O, Le Bras M, de Thé H. 2015. PML IV/ARF interaction enhances p53 SUMO-1 conjugation, activation, and senescence. Proc Natl Acad Sci U S A 112:14278–14283. https://doi.org/10.1073/pnas.1507540112.
37. Lunardi A, Gaboli M, Giorgio M, Rivi R, Bygrave A, Antoniou M, Drabek D, Dzierzak E, Fagioli M, Salmena L, Botto M, Cordon-Cardo C, Luzzatto L, Pelicci PG, Grosveld F, Pandolfi PP. 2011. A role for PML in innate immunity. Genes Cancer 2:10–19. https://doi.org/10.1177/1947601911402682.
38. Lecuit M, Dramsi S, Gottardi C, Fedor-Chaiken M, Gumbiner B, Cossart P. 1999. A single amino acid in E-cadherin responsible for host specificity towards the human pathogen *Listeria monocytogenes*. EMBO J 18:3956–3963. https://doi.org/10.1093/emboj/18.14.3956.
39. Bécavin C, Bouchier C, Lechat P, Archambaud C, Creno S, Gouin E, Wu Z, Kühbacher A, Brisse S, Pucciarelli MG, García-del Portillo F, Hain T, Portnoy DA, Chakraborty T, Lecuit M, Pizarro-Cerdá J, Moszer I, Bierne H, Cossart P. 2014. Comparison of widely used *Listeria monocytogenes* strains EGD, 10403S, and EGD-e highlights genomic variations underlying differences in pathogenicity. mBio 5:e00969-14. https://doi.org/10.1128/mBio.00969-14.
40. Lecuit M, Sonnenburg JL, Cossart P, Gordon JI. 2007. Functional genomic studies of the intestinal response to a foodborne enteropathogen in a humanized gnotobiotic mouse model. J Biol Chem 282:15065–15072. https://doi.org/10.1074/jbc.M610926200.
41. Portnoy DA, Jacks PS, Hinrichs DJ. 1988. Role of hemolysin for the intracellular growth of *Listeria monocytogenes*. J Exp Med 167:1459–1471. https://doi.org/10.1084/jem.167.4.1459.
42. Zhu J, Koken MH, Quignon F, Chelbi-Alix MK, Degos L, Wang ZY, Chen Z, de Thé H. 1997. Arsenic-induced PML targeting onto nuclear bodies: implications for the treatment of acute promyelocytic leukemia. Proc Natl Acad Sci U S A 94:3978–3983. https://doi.org/10.1073/pnas.94.8.3978.
43. Zhang XW, Yan XJ, Zhou ZR, Yang FF, Wu ZY, Sun HB, Liang WX, Song

AX, Lallemand-Breitenbach V, Jeanne M, Zhang QY, Yang HY, Huang QH, Zhou GB, Tong JH, Zhang Y, Wu JH, Hu HY, de Thé H, Chen SJ, Chen Z. 2010. Arsenic trioxide controls the fate of the PML-RARalpha oncoprotein by directly binding PML. Science 328:240–243. https://doi.org/10.1126/science.1183424.

44. de Thé H, Le Bras M, Lallemand-Breitenbach V. 2012. The cell biology of disease: acute promyelocytic leukemia, arsenic, and PML bodies. J Cell Biol 198:11–21. https://doi.org/10.1083/jcb.201112044.
45. Sternsdorf T, Jensen K, Will H. 1997. Evidence for covalent modification of the nuclear dot-associated proteins PML and Sp100 by PIC1/SUMO-1. J Cell Biol 139:1621–1634. https://doi.org/10.1083/jcb.139.7.1621.
46. Stuurman N, de Jong L, van Driel R. 1992. Nuclear frameworks: concepts and operational definitions. Cell Biol Int Rep 16:837–852. https://doi.org/10.1016/S0309-1651(05)80026-8.
47. Bhakdi S, Martin E. 1991. Superoxide generation by human neutrophils induced by low doses of *Escherichia coli* hemolysin. Infect Immun 59:2955–2962.
48. Hamon MA, Ribet D, Stavru F, Cossart P. 2012. Listeriolysin O: the Swiss army knife of *Listeria*. Trends Microbiol 20:360–368. https://doi.org/10.1016/j.tim.2012.04.006.
49. Scherer M, Klingl S, Sevvana M, Otto V, Schilling EM, Stump JD, Müller R, Reuter N, Sticht H, Muller YA, Stamminger T. 2014. Crystal structure of cytomegalovirus IE1 Protein reveals targeting of TRIM family member PML via coiled-coil interactions. PLoS Pathog 10:e1004512. https://doi.org/10.1371/journal.ppat.1004512.
50. Choi YH, Bernardi R, Pandolfi PP, Benveniste EN. 2006. The promyelocytic leukemia protein functions as a negative regulator of IFN-gamma signaling. Proc Natl Acad Sci U S A 103:18715–18720. https://doi.org/10.1073/pnas.0604800103.
51. Ulbricht T, Alzrigat M, Horch A, Reuter N, von Mikecz A, Steimle V, Schmitt E, Krämer OH, Stamminger T, Hemmerich P. 2012. PML promotes MHC class II gene expression by stabilizing the class II transactivator. J Cell Biol 199:49–63. https://doi.org/10.1083/jcb.201112015.
52. Kim YE, Ahn JH. 2015. Positive role of promyelocytic leukemia protein in type I interferon response and its regulation by human cytomegalovirus. PLoS Pathog 11:e1004785. https://doi.org/10.1371/journal.ppat.1004785.
53. Chen Y, Wright J, Meng X, Leppard KN. 2015. Promyelocytic leukemia protein isoform II promotes transcription factor recruitment to activate interferon beta and interferon-responsive gene expression. Mol Cell Biol 35:1660–1672. https://doi.org/10.1128/MCB.01478-14.
54. El Asmi F, Maroui MA, Dutrieux J, Blondel D, Nisole S, Chelbi-Alix MK. 2014. Implication of PMLIV in both intrinsic and innate immunity. PLoS Pathog 10:e1003975. https://doi.org/10.1371/journal.ppat.1003975.
55. Scherer M, Stamminger T. 2016. Emerging role of PML nuclear bodies in innate immune signaling. J Virol 90:5850–5854 https://doi.org/10.1128/JVI.01979-15.
56. Rusinova I, Forster S, Yu S, Kannan A, Masse M, Cumming H, Chapman R, Hertzog PJ. 2013. Interferome v2.0: an updated database of annotated interferon-regulated genes. Nucleic Acids Res 41:D1040–D1046. https://doi.org/10.1093/nar/gks1215.
57. Henry R, Shaughnessy L, Loessner MJ, Alberti-Segui C, Higgins DE, Swanson JA. 2006. Cytolysin-dependent delay of vacuole maturation in macrophages infected with *Listeria monocytogenes*. Cell Microbiol 8:107–119. https://doi.org/10.1111/j.1462-5822.2005.00604.x.
58. Malet JK, Cossart P, Ribet D. 2016. Alteration of epithelial cell lysosomal integrity induced by bacterial cholesterol-dependent cytolysins. Cell Microbiol. https://doi.org/10.1111/cmi.12682.
59. Wang ZG, Delva L, Gaboli M, Rivi R, Giorgio M, Cordon-Cardo C, Grosveld F, Pandolfi PP. 1998. Role of PML in cell growth and the retinoic acid pathway. Science 279:1547–1551. https://doi.org/10.1126/science.279.5356.1547.
60. Kühbacher A, Cossart P, Pizarro-Cerdá J. 2014. Internalization assays for *Listeria monocytogenes*. Methods Mol Biol 1157:167–178. https://doi.org/10.1007/978-1-4939-0703-8_14.
61. Team RC. 2016. R: A language and environment for statistical computing. R Foundation for Statistical Computing, Vienna, Austria.
62. Ritchie ME, Phipson B, Wu D, Hu Y, Law CW, Shi W, Smyth GK. 2015. Limma powers differential expression analyses for RNA-sequencing and microarray studies. Nucleic Acids Res 43:e47. https://doi.org/10.1093/nar/gkv007.
63. Benjamini Y, Hochberg Y. 1995. Controlling the false discovery rate: a practical and powerful approach to multiple testing. J R Stat Soc B Stat Methodol 57:289–300.
64. Glomski IJ, Gedde MM, Tsang AW, Swanson JA, Portnoy DA. 2002. The *Listeria monocytogenes* hemolysin has an acidic pH optimum to compartmentalize activity and prevent damage to infected host cells. J Cell Biol 156:1029–1038. https://doi.org/10.1083/jcb.200201081.

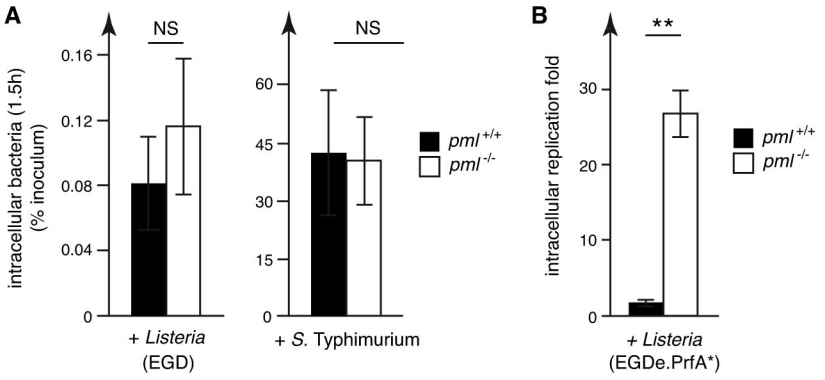

Figure S1 : PML restricts bacteria intracellular replication but not bacterial entry in MEFs. MEFs derived from *pml*$^{+/+}$ or *pml*$^{-/-}$ mice were infected by *L. monocytogenes* (EGD or EGDe.PrfA* strains) or *S.* Typhimurium. (A) Histograms correspond to the number of intracellular bacteria recovered after 1.5h of infection, expressed as the percentage of the inoculum initially used for infection (mean ± SEM from 6-8 independent experiments; NS, not significant; unpaired two-tailed Student's t-test). No significant differences were observed in bacteria numbers, suggesting that internalization efficiency of *Listeria* and *Salmonella* are similar in both *pml*$^{+/+}$ or *pml*$^{-/-}$ MEFs. (B) Histograms correspond to bacteria intracellular replication folds, expressed as the ratio of intracellular bacteria at 24h versus 1.5h of infection (mean ± s.d. from 3 independent experiments; **P<0.01; unpaired two-tailed Student's t-test). A significant increase in the replication fold efficiency is observed in *pml*$^{-/-}$ compared to *pml*$^{+/+}$ MEFs indicating that PML restricts intracellular replication of *Listeria* EGDe.PrfA* strain.

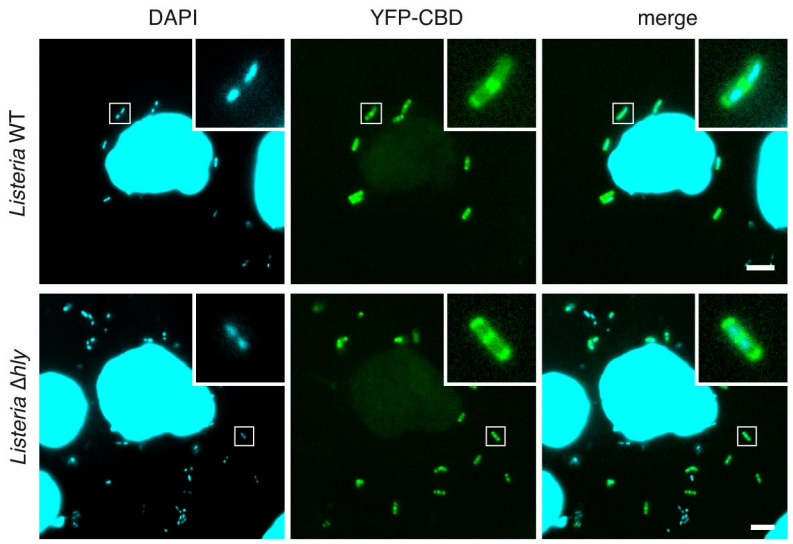

Figure S2 : Detection of *Listeria* vacuolar escape in MEFs. Immunofluorescence analysis of *pml*$^{+/+}$ MEFs transfected with an expression vector for YFP-CBD, a YFP chimera protein of the cell-wall binding domain from the *Listeria* phage endolysin Ply118 (R. Henry, L. Shaughnessy, M.J. Loessner, C. Alberti-Segui, D.E. Higgins and J.A. Swanson, Cell Microbiol 8:107-119, 2006, doi:10.1111/j.1462-5822.2005.00604.x). MEFs were infected 24h after transfection with wild-type or Δ*hly Listeria monocytogenes*. After 1 hour of infection, cells were washed and incubated for additional four hours in culture media supplemented with gentamicin to kill extracellular bacteria, while intracellular bacteria remain unaffected by this antibiotic. Cells were then fixed and bacterial and cellular DNA were stained with DAPI (scale bar, 5 µm). The YFP-CBD protein, synthetized in the host cell cytoplasm, recognize and bind only to bacteria that escaped from the internalization vacuole. Here, CBD-positive Δ*hly Listeria* can be detected, indicating that at least a fraction of these bacteria can escape the internalization vacuole in this murine cell line and reach the host cell cytosol, as already observed for several human cell lines (M.A. Hamon, D. Ribet, F. Stavru and P. Cossart, Trends Microbiol 20:360-368, 2012, doi:10.1016/j.tim.2012.04.006).

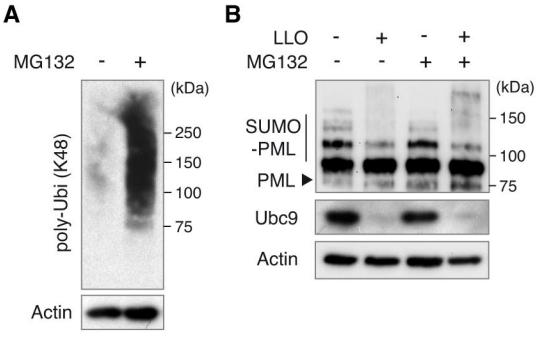

Figure S3 : LLO induces PML deSUMOylation rather than degradation. (A) Immunoblot analysis using anti-K48-linked polyubiquitin and anti-actin antibodies of whole-cell lysates from CHO-PML cells pre-incubated with 10 µM MG132 for 5h. The level of proteins conjugated to K48-polyubiquitin chains increased after MG132 treatment, thus validating proteasome inhibition in these conditions. (B) Immunoblot analysis using anti-PML, anti-Ubc9 and anti-actin antibodies of whole-cell lysates from CHO-PML cells pre-incubated with 10 µM MG132 for 5h and then treated with 1 nM LLO for 20 min. Pre-treatment with MG132 does not block loss of PML SUMOylated forms, suggesting that LLO triggers PML deSUMOylation rather than degradation.

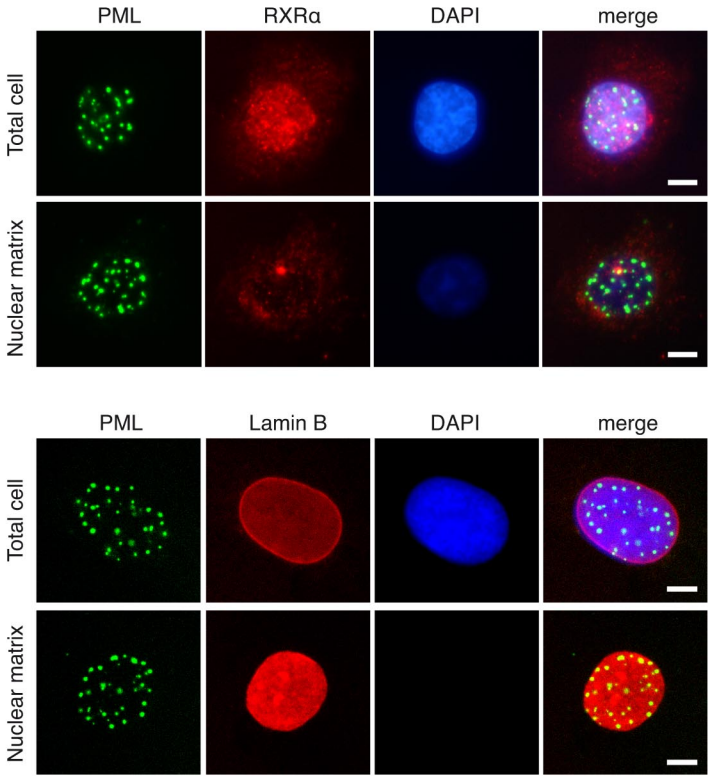

Figure S4 : Control of *in situ* nuclear matrix preparations. Immunofluorescence analysis of total nuclei from CHO-PML cells or nuclear matrix preparations using DAPI, anti-PML, anti-Lamin B and anti-RXRα antibodies. As expected, after the high salt extraction and nuclease treatment used for nuclear matrix preparation, the nuclear soluble RXRα factor and DNA were removed, whereas Lamin B and NB associated-PML, which belong to the nuclear matrix fraction, are still present. Scale bar, 5 µm.

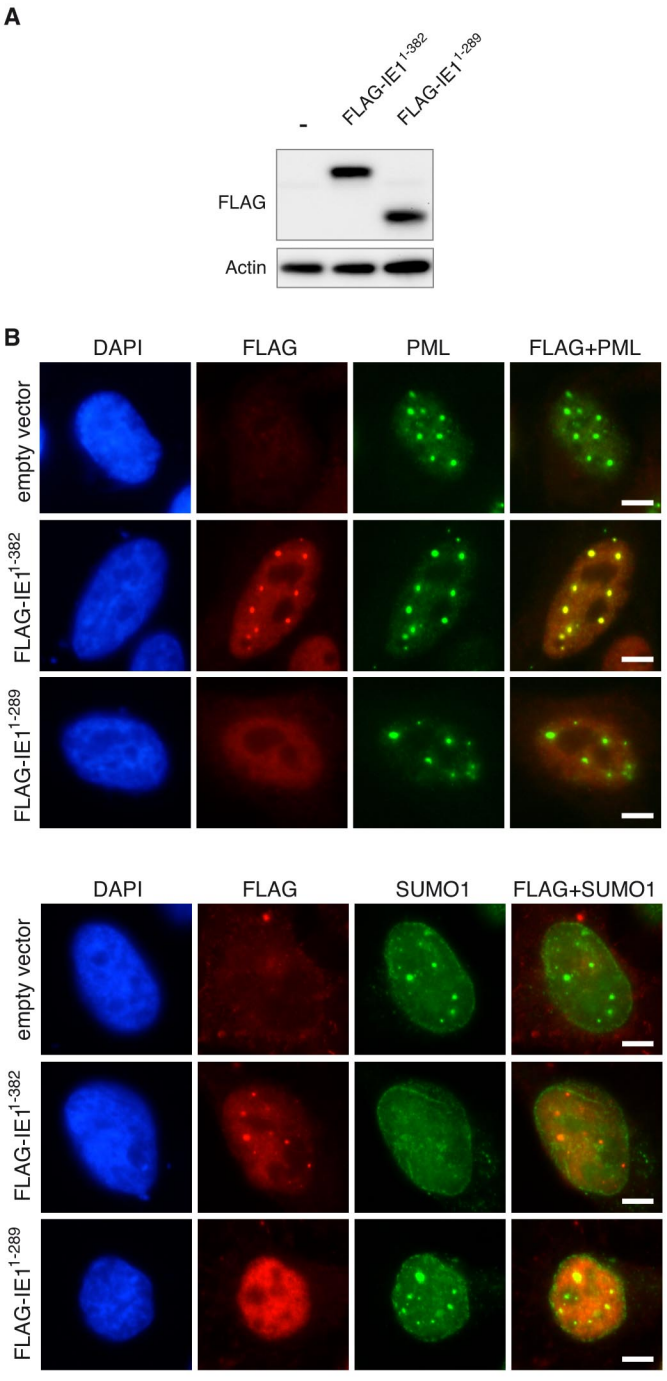

Figure S5 : hCMV iE1$^{1-382}$ protein binds to PML and induces its deSUMOylation. (A) Immunoblot analysis using anti-FLAG and anti-actin antibodies of HeLa cells transfected with empty vector or expression vectors for FLAG-iE1$^{1-382}$ or iE1$^{1-289}$. (B) Immunofluorescence analysis of nuclei from transfected HeLa cells stained with DAPI, anti-FLAG, anti-PML and anti-SUMO1 antibodies. The iE1$^{1-382}$ protein displays a nuclear localisation, binds to PML and induces its deSUMOylation. The iE1$^{1-289}$ protein also has a nuclear localisation but does not bind nor deSUMOylate PML. Scale bar, 5 µm.

Table S1A : Relative gene expression levels in *pml*$^{-/-}$ versus *pml*$^{+/+}$ MEFs after infection with wild-type *Listeria.*

Gene expression was determined by quantitative PCR (qPCR) analysis of RNAs from *pml*$^{-/-}$ and *pml*$^{+/+}$ MEFs infected for 24 h with wild-type *Listeria.* Data represent fold changes of gene expression levels in *pml*$^{-/-}$ MEFs compared to the levels in *pml*$^{+/+}$ MEFs (mean results from 4 independent experiments). Genes that had fold changes with an adjusted *P* value of <0.05 (Benjamini and Hochberg method) are considered differentially regulated between the two conditions being compared.

Symbol	Unigene	Refseq	Description	fold change	adj. p-value
Akt1	Mm.6645	NM_009652	Thymoma viral proto-oncogene 1	0,805647919	0,449896502
Apcs	Mm.330510	NM_011318	Serum amyloid P-component	0,967329903	0,802082863
Birc3	Mm.2026	NM_007464	Baculoviral IAP repeat-containing 3	0,291520208	0,005448087
Bpi	Mm.260883	NM_177850	Bactericidal permeablility increasing protein	0,967329903	0,802082863
Camp	Mm.3834	NM_009921	Cathelicidin antimicrobial peptide	0,051746532	0,000284145
Card6	Mm.31252	NM_001163138	Caspase recruitment domain family, member 6	0,851589058	0,760067154
Card9	Mm.330064	NM_001037747	Caspase recruitment domain family, member 9	0,710495416	0,451016024
Casp1	Mm.1051	NM_009807	Caspase 1	0,207715982	0,026880893
Casp8	Mm.336851	NM_009812	Caspase 8	0,924355892	0,563882338
Ccl3	Mm.1282	NM_011337	Chemokine (C-C motif) ligand 3	0,121384701	0,046442805
Ccl4	Mm.244263	NM_013652	Chemokine (C-C motif) ligand 4	19,15982731	0,031227479
Ccl5	Mm.284248	NM_013653	Chemokine (C-C motif) ligand 5	0,49785163	0,330300674
Cd14	Mm.3460	NM_009841	CD14 antigen	0,536505356	0,028054009
Chuk	Mm.3996	NM_007700	Conserved helix-loop-helix ubiquitous kinase	0,881339559	0,374460882
Crp	Mm.28767	NM_007768	C-reactive protein, pentraxin-related	0,967329903	0,802082863
Ctsg	Mm.4858	NM_007800	Cathepsin G	0,967329903	0,802082863
Cxcl1	Mm.21013	NM_008176	Chemokine (C-X-C motif) ligand 1	0,230924465	0,041167486
Cxcl3	Mm.244289	NM_203320	Chemokine (C-X-C motif) ligand 3	0,115746575	0,050390158
Dmbt1	Mm.4138	NM_007769	Deleted in malignant brain tumors 1	0,967329903	0,802082863
Fadd	Mm.5126	NM_010175	Fas (TNFRSF6)-associated via death domain	0,892773194	0,517329563
Hsp90aa1	Mm.1843	NM_010480	Heat shock protein 90, alpha (cytosolic), class A member 1	1,294716536	0,125045859
Ifna9	Mm.377092	NM_010507	Interferon alpha 9	1,860352616	0,354283729
Ifnb1	Mm.1245	NM_010510	Interferon beta 1, fibroblast	14,36576446	0,070640443
Ikbkb	Mm.277886	NM_010546	Inhibitor of kappaB kinase beta	0,901983914	0,484343709
Il12a	Mm.103783	NM_008351	Interleukin 12A	0,967329903	0,802082863
Il12b	Mm.239707	NM_008352	Interleukin 12B	0,777180335	0,563882338
Il18	Mm.1410	NM_008360	Interleukin 18	0,218741451	3,86E-05
Il1b	Mm.222830	NM_008361	Interleukin 1 beta	0,704721506	0,3931557
Il6	Mm.1019	NM_031168	Interleukin 6	0,478230436	0,368900936
Irak1	Mm.38241	NM_008363	Interleukin-1 receptor-associated kinase 1	0,702034863	0,050390158
Irak3	Mm.146194	NM_028679	Interleukin-1 receptor-associated kinase 3	0,288607921	0,00276169
Irf5	Mm.6479	NM_012057	Interferon regulatory factor 5	1,486748742	0,451016024
Irf7	Mm.3233	NM_016850	Interferon regulatory factor 7	0,518307383	0,028054009
Jun	Mm.275071	NM_010591	Jun oncogene	0,823854644	0,318234804
Lbp	Mm.218846	NM_008489	Lipopolysaccharide binding protein	0,426759077	0,041167486
Lcn2	Mm.9537	NM_008491	Lipocalin 2	0,025004776	0,000768299
Ltf	Mm.282359	NM_008522	Lactotransferrin	0,227327583	0,0617896
Ly96	Mm.116844	NM_016923	Lymphocyte antigen 96	0,917559202	0,670325576
Lyz2	Mm.45436	NM_017372	Lysozyme 2	0,164677867	0,008007379
Map2k1	Mm.248907	NM_008927	Mitogen-activated protein kinase kinase 1	1,253104061	0,182488087
Map2k3	Mm.18494	NM_008928	Mitogen-activated protein kinase kinase 3	0,667513887	0,070640443
Map2k4	Mm.412922	NM_009157	Mitogen-activated protein kinase kinase 4	0,991761514	0,933968547
Map3k7	Mm.258589	NM_172688	Mitogen-activated protein kinase kinase kinase 7	0,738156959	0,051101919
Mapk1	Mm.196581	NM_011949	Mitogen-activated protein kinase 1	0,789899729	0,041167486
Mapk14	Mm.311337	NM_011951	Mitogen-activated protein kinase 14	0,681216082	0,028054009
Mapk3	Mm.8385	NM_011952	Mitogen-activated protein kinase 3	0,832931632	0,35703465
Mapk8	Mm.21495	NM_016700	Mitogen-activated protein kinase 8	1,279865571	0,054664413
Mefv	Mm.143718	NM_019453	Mediterranean fever	0,686885621	0,35703465
Mpo	Mm.4668	NM_010824	Myeloperoxidase	34,08073764	5,27E-09
Myd88	Mm.213003	NM_010851	Myeloid differentiation primary response gene 88	0,521745301	0,056705919
Naip1	Mm.6898	NM_008670	NLR family, apoptosis inhibitory protein 1	0,967329903	0,802082863
Nfkb1	Mm.256765	NM_008689	Nuclear factor of kappa light polypeptide gene enhancer in B-cells 1, p105	0,568717753	0,050390158
Nfkbia	Mm.170515	NM_010907	Nuclear factor of kappa light polypeptide gene enhancer in B-cells inhibitor, alpha	0,425624882	0,042584974
Nlrc4	Mm.311884	NM_001033367	NLR family, CARD domain containing 4	0,967329903	0,802082863
Nlrp1a	Mm.240227	NM_001004142	NLR family, pyrin domain containing 1A	0,967329903	0,802082863
Nlrp3	Mm.54174	NM_145827	NLR family, pyrin domain containing 3	0,069477589	0,029970424
Nod1	Mm.28498	NM_172729	Nucleotide-binding oligomerization domain containing 1	0,62331168	0,074243304
Nod2	Mm.222633	NM_145857	Nucleotide-binding oligomerization domain containing 2	0,122525033	0,003947975
Pik3ca	Mm.260521	NM_008839	Phosphatidylinositol 3-kinase, catalytic, alpha polypeptide	0,697445473	0,04010536
Prtn3	Mm.2364	NM_011178	Proteinase 3	0,905161886	0,563882338
Pstpip1	Mm.2534	NM_011193	Proline-serine-threonine phosphatase-interacting protein 1	1,144889032	0,35703465
Pycard	Mm.24163	NM_023258	PYD and CARD domain containing	0,686349037	0,133313657
Rac1	Mm.292510	NM_009007	RAS-related C3 botulinum substrate 1	0,82280629	0,135401393
Rela	Mm.249966	NM_009045	V-rel reticuloendotheliosis viral oncogene homolog A (avian)	0,757600671	0,075564821
Ripk1	Mm.374799	NM_009068	Receptor (TNFRSF)-interacting serine-threonine kinase 1	0,805230051	0,074243304
Ripk2	Mm.112765	NM_138952	Receptor (TNFRSF)-interacting serine-threonine kinase 2	0,3307416	0,037184013
Slc11a1	Mm.2913	NM_013612	Solute carrier family 11 (proton-coupled divalent metal ion transporters), member 1	0,338993954	0,004856211
Slpi	Mm.371583	NM_011414	Secretory leukocyte peptidase inhibitor	0,070662562	0,000521699
Sugt1	Mm.18972	NM_026474	SGT1, suppressor of G2 allele of SKP1 (S. cerevisiae)	1,028680036	0,802082863
Ticam1	Mm.203952	NM_174989	Toll-like receptor adaptor molecule 1	0,688093557	0,028054009
Ticam2	Mm.149280	NM_173394	Toll-like receptor adaptor molecule 2	2,464044803	0,171670799
Tirap	Mm.23987	NM_054096	Toll-interleukin 1 receptor (TIR) domain-containing adaptor protein	0,957443176	0,802082863
Tlr1	Mm.273024	NM_030682	Toll-like receptor 1	0,332704992	0,050390158
Tlr2	Mm.87596	NM_011905	Toll-like receptor 2	0,174159689	0,020134674
Tlr4	Mm.38049	NM_021297	Toll-like receptor 4	0,750227555	0,041167486
Tlr5	Mm.116894	NM_016928	Toll-like receptor 5	2,216295974	0,145777458
Tlr6	Mm.42146	NM_011604	Toll-like receptor 6	0,115246226	0,000521699

Tlr9	Mm.44889	NM_031178	Toll-like receptor 9	0,967329903	0,802082863
Tnf	Mm.1293	NM_013693	Tumor necrosis factor	0,070423439	0,051101919
Tnfrsf1a	Mm.1258	NM_011609	Tumor necrosis factor receptor superfamily, member 1a	0,687927009	0,050390158
Tollip	Mm.103551	NM_023764	Toll interacting protein	1,141639945	0,41205087
Traf6	Mm.292729	NM_009424	Tnf receptor-associated factor 6	1,129453159	0,339656244
Xiap	Mm.259879	NM_009688	X-linked inhibitor of apoptosis	0,810923309	0,071119149
Zbp1	Mm.116687	NM_021394	Z-DNA binding protein 1	0,671835129	0,318234804
Actb	Mm.328431	NM_007393	Actin, beta	1,124913073	0,335674456
B2m	Mm.163	NM_009735	Beta-2 microglobulin	0,760343937	0,156351593
Gapdh	Mm.309092	NM_008084	Glyceraldehyde-3-phosphate dehydrogenase	1,084382535	0,58656136
Gusb	Mm.3317	NM_010368	Glucuronidase, beta	0,856552877	0,350460562
Hsp90ab1	Mm.2180	NM_008302	Heat shock protein 90 alpha (cytosolic), class B member 1	1,258736922	0,125045859

Table S1B : Relative gene expression levels in *pml*$^{-/-}$ versus *pml*$^{+/+}$ MEFs after infection with a Δ*hly Listeria* mutant.

Gene expression was determined by qPCR analysis of RNAs from *pml*$^{-/-}$ and *pml*$^{+/+}$ MEFs infected for 24 h with a Δ*hly Listeria* mutant. Data represent fold changes of gene expression levels in *pml*$^{-/-}$ MEFs compared to the levels in *pml*$^{+/+}$ MEFs (mean results from 4 independent experiments). Genes that had fold changes with an adjusted *P* value of <0.05 (Benjamini and Hochberg method) are considered differentially regulated between the two conditions being compared.

Symbol	Unigene	Refseq	Description	fold change	adj. p-value
Akt1	Mm.6645	NM_009652	Thymoma viral proto-oncogene 1	0,7747379	0,39628526
Apcs	Mm.330510	NM_011318	Serum amyloid P-component	1,047651598	0,745582353
Birc3	Mm.2026	NM_007464	Baculoviral IAP repeat-containing 3	0,385708893	0,01507407
Bpi	Mm.260883	NM_177850	Bactericidal permeablility increasing protein	1,047651598	0,745582353
Camp	Mm.3834	NM_009921	Cathelicidin antimicrobial peptide	0,068185426	0,000416505
Card6	Mm.31252	NM_001163138	Caspase recruitment domain family, member 6	0,549083326	0,189724905
Card9	Mm.330064	NM_001037747	Caspase recruitment domain family, member 9	2,041608191	0,128597352
Casp1	Mm.1051	NM_009807	Caspase 1	0,151577811	0,00593596
Casp8	Mm.336851	NM_009812	Caspase 8	1,102452475	0,507142094
Ccl3	Mm.1282	NM_011337	Chemokine (C-C motif) ligand 3	0,018973032	0,001729062
Ccl4	Mm.244263	NM_013652	Chemokine (C-C motif) ligand 4	0,371803024	0,440480068
Ccl5	Mm.284248	NM_013653	Chemokine (C-C motif) ligand 5	0,082453329	0,003396078
Cd14	Mm.3460	NM_009841	CD14 antigen	0,630268075	0,065795541
Chuk	Mm.3996	NM_007700	Conserved helix-loop-helix ubiquitous kinase	1,120027565	0,461181622
Crp	Mm.28767	NM_007768	C-reactive protein, pentraxin-related	1,047651598	0,745582353
Ctsg	Mm.4858	NM_007800	Cathepsin G	1,047651598	0,745582353
Cxcl1	Mm.21013	NM_008176	Chemokine (C-X-C motif) ligand 1	0,17884403	0,016100201
Cxcl3	Mm.244289	NM_203320	Chemokine (C-X-C motif) ligand 3	0,075953539	0,019215159
Dmbt1	Mm.4138	NM_007769	Deleted in malignant brain tumors 1	1,047651598	0,745582353
Fadd	Mm.5126	NM_010175	Fas (TNFRSF6)-associated via death domain	1,221721404	0,261382172
Hsp90aa1	Mm.1843	NM_010480	Heat shock protein 90, alpha (cytosolic), class A member 1	1,130442674	0,498174993
Ifna9	Mm.377092	NM_010507	Interferon alpha 9	1,016154508	0,973653676
Ifnb1	Mm.1245	NM_010510	Interferon beta 1, fibroblast	0,184566955	0,253631319
Ikbkb	Mm.277886	NM_010546	Inhibitor of kappaB kinase beta	0,730930712	0,045591905
Il12a	Mm.103783	NM_008351	Interleukin 12A	1,047651598	0,745582353
Il12b	Mm.239707	NM_008352	Interleukin 12B	0,450981866	0,07870416
Il18	Mm.1410	NM_008360	Interleukin 18	0,187554257	1,39E-05
Il1b	Mm.222830	NM_008361	Interleukin 1 beta	0,810928823	0,677629818
Il6	Mm.1019	NM_031168	Interleukin 6	0,065042448	0,005618169
Irak1	Mm.38241	NM_008363	Interleukin-1 receptor-associated kinase 1	1,190719881	0,318127932
Irak3	Mm.146194	NM_028679	Interleukin-1 receptor-associated kinase 3	0,318570543	0,003396078
Irf5	Mm.6479	NM_012057	Interferon regulatory factor 5	1,049410302	0,924550557
Irf7	Mm.3233	NM_016850	Interferon regulatory factor 7	0,294034794	0,000719952
Jun	Mm.275071	NM_010591	Jun oncogene	0,546812718	0,00593596
Lbp	Mm.218846	NM_008489	Lipopolysaccharide binding protein	0,336464943	0,010486189
Lcn2	Mm.9537	NM_008491	Lipocalin 2	0,01750443	0,000416505
Ltf	Mm.282359	NM_008522	Lactotransferrin	0,135044302	0,017294324
Ly96	Mm.116844	NM_016923	Lymphocyte antigen 96	0,719026086	0,0926678
Lyz2	Mm.45436	NM_017372	Lysozyme 2	0,359543783	0,068596433
Map2k1	Mm.248907	NM_008927	Mitogen-activated protein kinase kinase 1	0,754530427	0,105149544
Map2k3	Mm.18494	NM_008928	Mitogen-activated protein kinase kinase 3	1,08176576	0,745582353
Map2k4	Mm.412922	NM_009157	Mitogen-activated protein kinase kinase 4	1,052467814	0,736187512
Map3k7	Mm.258589	NM_172688	Mitogen-activated protein kinase kinase kinase 7	0,895417641	0,498174993
Mapk1	Mm.196581	NM_011949	Mitogen-activated protein kinase 1	1,076581289	0,507142094
Mapk14	Mm.311337	NM_011951	Mitogen-activated protein kinase 14	1,06139874	0,745582353
Mapk3	Mm.8385	NM_011952	Mitogen-activated protein kinase 3	1,249469958	0,261382172
Mapk8	Mm.21495	NM_016700	Mitogen-activated protein kinase 8	1,077159379	0,59617218
Mefv	Mm.143718	NM_019453	Mediterranean fever	0,461571538	0,065795541
Mpo	Mm.4668	NM_010824	Myeloperoxidase	61,26062717	1,04E-09
Myd88	Mm.213003	NM_010851	Myeloid differentiation primary response gene 88	0,428456355	0,01799863
Naip1	Mm.6898	NM_008670	NLR family, apoptosis inhibitory protein 1	1,047651598	0,745582353
Nfkb1	Mm.256765	NM_008689	Nuclear factor of kappa light polypeptide gene enhancer in B-cells 1, p105	0,513097535	0,021266439
Nfkbia	Mm.170515	NM_010907	Nuclear factor of kappa light polypeptide gene enhancer in B-cells inhibitor, alpha	0,32224085	0,010486189
Nlrc4	Mm.311884	NM_001033367	NLR family, CARD domain containing 4	1,047651598	0,745582353
Nlrp1a	Mm.240227	NM_001004142	NLR family, pyrin domain containing 1A	1,047651598	0,745582353
Nlrp3	Mm.54174	NM_145827	NLR family, pyrin domain containing 3	0,05702897	0,01508063
Nod1	Mm.28498	NM_172729	Nucleotide-binding oligomerization domain containing 1	0,645407162	0,104378302
Nod2	Mm.222633	NM_145857	Nucleotide-binding oligomerization domain containing 2	0,207142906	0,01216257
Pik3ca	Mm.260521	NM_008839	Phosphatidylinositol 3-kinase, catalytic, alpha polypeptide	0,859564533	0,342926445
Prtn3	Mm.2364	NM_011178	Proteinase 3	1,047651598	0,756522538
Pstpip1	Mm.2534	NM_011193	Proline-serine-threonine phosphatase-interacting protein 1	1,968289277	0,00080719
Pycard	Mm.24163	NM_023258	PYD and CARD domain containing	1,109642579	0,745582353
Rac1	Mm.292510	NM_009007	RAS-related C3 botulinum substrate 1	0,900285668	0,456795968
Rela	Mm.249966	NM_009045	V-rel reticuloendotheliosis viral oncogene homolog A (avian)	0,520798809	0,001591794
Ripk1	Mm.374799	NM_009068	Receptor (TNFRSF)-interacting serine-threonine kinase 1	0,844729507	0,170836006
Ripk2	Mm.112765	NM_138952	Receptor (TNFRSF)-interacting serine-threonine kinase 2	0,241260979	0,008392059
Slc11a1	Mm.2913	NM_013612	Solute carrier family 11 (proton-coupled divalent metal ion transporters), member 1	0,654865622	0,167325753
Slpi	Mm.371583	NM_011414	Secretory leukocyte peptidase inhibitor	0,016524389	1,39E-05
Sugt1	Mm.18972	NM_026474	SGT1, suppressor of G2 allele of SKP1 (S. cerevisiae)	1,172229871	0,129492135
Ticam1	Mm.203952	NM_174989	Toll-like receptor adaptor molecule 1	1,096450968	0,569403791
Ticam2	Mm.149280	NM_173394	Toll-like receptor adaptor molecule 2	4,005553242	0,046609022
Tirap	Mm.23987	NM_054096	Toll-interleukin 1 receptor (TIR) domain-containing adaptor protein	1,242225184	0,231111357
Tlr1	Mm.273024	NM_030682	Toll-like receptor 1	0,478376019	0,170836006
Tlr2	Mm.87596	NM_011905	Toll-like receptor 2	0,249681147	0,031575046
Tlr4	Mm.38049	NM_021297	Toll-like receptor 4	1,011339133	0,924550557
Tlr5	Mm.116894	NM_016928	Toll-like receptor 5	7,060499758	0,004036422
Tlr6	Mm.42146	NM_011604	Toll-like receptor 6	0,233400925	0,004205693

Tlr9	Mm.44889	NM_031178	Toll-like receptor 9	1,047651598	0,745582353
Tnf	Mm.1293	NM_013693	Tumor necrosis factor	0,03776951	0,019215159
Tnfrsf1a	Mm.1258	NM_011609	Tumor necrosis factor receptor superfamily, member 1a	0,693362328	0,052690971
Tollip	Mm.103551	NM_023764	Toll interacting protein	1,095318756	0,634335459
Traf6	Mm.292729	NM_009424	Tnf receptor-associated factor 6	0,863050757	0,242434983
Xiap	Mm.259879	NM_009688	X-linked inhibitor of apoptosis	0,807567507	0,068596433
Zbp1	Mm.116687	NM_021394	Z-DNA binding protein 1	0,205761975	0,001591794
Actb	Mm.328431	NM_007393	Actin, beta	1,363884888	0,016100201
B2m	Mm.163	NM_009735	Beta-2 microglobulin	0,821458112	0,329383359
Gapdh	Mm.309092	NM_008084	Glyceraldehyde-3-phosphate dehydrogenase	0,949481714	0,745582353
Gusb	Mm.3317	NM_010368	Glucuronidase, beta	0,995505906	0,973653676
Hsp90ab1	Mm.2180	NM_008302	Heat shock protein 90 alpha (cytosolic), class B member 1	0,944288658	0,745582353

Table S2A : Relative cytokine production levels in *pml*$^{-/-}$ versus *pml*$^{+/+}$ MEFs after infection with wild-type *Listeria.*

Cytokine production was quantified using supernatants from *pml*$^{-/-}$ and *pml*$^{+/+}$ MEFs infected for 24 h with wild-type *Listeria.* Data represent fold changes of cytokine production levels in *pml*$^{-/-}$ MEFs compared to the levels in *pml*$^{+/+}$ MEFs (mean results from 3 independent experiments). Cytokines that had fold changes with an adjusted *P* value of <0.05 (Benjamini and Hochberg method) are considered differentially produced between the two conditions being compared.

Description	Entrez Gene ID	Alternative nomenclature	fold change	adj. p-value
Adiponectin/Acrp30	11450	AdipoQ	0,912953786	0,84520897
Amphiregulin	11839	AR, SDGF	0,693013084	0,633530753
Angiopoietin-1	11600	Ang-1, Angpt1	1,023590674	0,934641044
Angiopoietin-2	11601	Ang-2, Angpt2	0,859603528	0,616892132
Angiopoietin-like 3	30924	ANGPT-L3	0,906591825	0,778538312
BAFF/BLyS/TNFSF13B	24099	CD257, TALL1, THANK, ZTNF4	0,373994862	0,024252989
C-reactive Protein/CRP	12944		0,643209672	0,702917165
C1qR1/CD93	17064	AA4, Antigen C1qRp, CD93	0,937820844	0,876318279
CCL11/Eotaxin	20292		0,914478824	0,778538312
CCL12/MCP-5	20293		1,239675213	0,702917165
CCL17/TARC	20295		1,202598199	0,717468806
CCL19/MIP-3beta	24047	ELC	0,655029265	0,118538101
CCL2/JE/MCP-1	20296	MCAF	0,827330796	0,443942399
CCL20/MIP-3alpha	20297	exodus-1, LARC	0,054257837	0,024546156
CCL21/6Ckine	18829	exodus-2, SCYA21, SLC, TCA-4	0,672449183	0,330976139
CCL22/MDC	20299	ABCD-1, MDC, STCP-1	1,302290262	0,602407675
CCL3/CCL4/MIP-1alpha/beta	20302/20303		1,323536052	0,451732875
CCL5/RANTES	20304	SISd	0,999929661	0,999666391
CCL6/C10	20305	MRP-1	0,945726998	0,907052945
CD14	12475		0,491054613	0,557918711
CD160	54215	Natural killer cell receptor BY55, NK1, NK28	0,92665823	0,880663794
CD40/TNFRSF5	21939		1,9534616	0,645610823
Chemerin	71660	RARRES2, TIG-2	0,863376075	0,645610823
Chitinase 3-like 1	12654	CHI3L1, Cgp39, YKL40	0,254040285	0,087301651
Coagulation Factor III/Tissue Factor	14066	TF, CD142, Thromboplastin	0,520476338	0,056305229
Complement component C5/C5a	15139	C5/C5a	0,94171242	0,880663794
Complement Factor D	11537	Adipsin, C3 convertase activator, Properdin factor D	0,281156783	1,15E-01
CX3CL1/Fractalkine	20312	FKN, Neurotactin	0,517030189	0,038582431
CXCL1/KC	14825	CINC-1, GRO alpha, KC, MGSA-alpha	0,485457322	0,069461943
CXCL10/IP-10	15945	CRG-2, C7	0,769244457	0,602407675
CXCL11/I-TAC	56066	H174, SCYB9B	0,073650352	0,074510558
CXCL13/BLC/BCA-1	55985		0,702490744	0,395917456
CXCL16	66102	SRPSOX	0,505631543	0,28189703
CXCL2/MIP-2	20310	GRO-beta	0,334846813	0,44939113
CXCL9/MIG	17329	CRG-10	0,82423848	0,635118571
Cystatin C	13010	ARMD11, CST3, Gamma-trae-ce	0,871662097	0,61665454
DKK-1	13380	Dickkopf-1	0,694609192	0,294566344
DPPIV/CD26	13482	Dpp4, Dipeptidyl-peptidase IV	0,797785088	0,611241681
E-Selectin/CD62E	20339	ELAM1, LECAM2, Sele	1,448089722	0,437301383
EGF	13645	Epidermal Growth Factor	1,084361694	0,778538312
Endoglin/CD105	13805	ENG	0,819716103	0,667271909
Endostatin	12822	Col18a1	0,306920068	0,015279373
Fetuin A/AHSG	11625	AHSG, alpha-2-HS-glycoprotein	0,619141803	0,301194787
FGF acidic	14164	FGF-1	1,052216619	9,09E-01
FGF-21	56636		0,746214327	0,667271909
Flt-3 Ligand	14256	Flt3lg	4,363028765	0,024252989
G-CSF	12985	Csf3	0,557703129	0,087301651
Gas 6	14456	Growth Arrest Specific	0,70825806	0,501610842
GDF-15	23886	MIC-1	0,876309674	0,717468806
GM-CSF	12981	Csf2	0,594155732	0,667271909
HGF	15234	Scatter Factor, SF, Hepatopoietin-A	1,571479907	0,294566344
ICAM-1/CD54	15894		0,842133478	0,706242094
IFN-gamma	15978	IFNG	0,932774095	0,876318279
IGFBP-1	16006		1,662773326	0,633530753
IGFBP-2	16008		0,018677808	0,000117846
IGFBP-3	16009		0,893372754	0,842340565
IGFBP-5	16011		0,756519572	0,61665454
IGFBP-6	16012		0,101504581	0,020108119
IL-10	16153	CSIF	1,087686689	0,842340565
IL-11	16156		0,687774894	0,557918711
IL-12p40	16160		0,637700527	0,150103296
IL-13	16163		1,288051442	0,501610842
IL-15	16168		0,699710907	0,370433104
IL-17A	16171		0,162322933	0,399910173
IL-1alpha/IL-1F1	16175		0,679688334	0,155423704
IL-1beta/IL-1F2	16176		0,713876529	0,137997571
IL-1ra/IL-1F3	16181	IL1RN	0,702407338	0,114515872
IL-2	16183		0,550153345	0,658799304
IL-22	50929	IL-TIF	1,107588032	0,778538312
IL-23	83430		0,623013452	0,114515872
IL-27p28	246779		0,749616553	0,557918711
IL-28A/B	330496/338374		0,740736389	0,384938916
IL-3	16187		0,744398765	0,682266048
IL-33	77125	NF HEV, DVS 27	0,403793259	0,056305229
IL-4	16189	B cell-stimulatory factor-1	0,886973559	0,667271909
IL-5	16191		0,800410911	0,611241681

IL-6	16193		0,40206527	0,587089397
IL-7	16196		0,530353063	0,087301651
LDL R	16835	low density lipoprotein receptor	0,949715303	0,925627231
Leptin	16846	OB	0,865921754	0,658799304
LIF	16878		0,428507339	0,082255021
Lipocalin-2/NGAL	16819	Siderocalin, 24p3	0,055608953	0,028584464
LIX	20311	CXCL5, GCP-2, ENA-78	0,10757854	0,069461943
M-CSF	12977	CSF-1	0,944390319	0,880663794
MMP-2	17390	Gelatinase A	0,634178354	0,350202708
MMP-3	17392	Stromelysin-1	0,004034201	0,0000054
MMP-9	17395	Clg4b, Gelatinase B, GELB	0,305018498	0,044353604
Myeloperoxidase	17523	MPO	0,515732308	0,222634843
Osteopontin (OPN)	20750	Eta-1, Spp1	0,823309402	0,61665454
Osteoprotegerin/TNFRSF11B	18383	OPG, Ocif	0,865347539	0,778538312
P-Selectin/CD62P	20344	GMP-140, LECAM3, Selep	1,241396357	0,633530753
PD-ECGF/Thymidine phosphorylase	72962	dThdPase, ECGF1, Gliostatin, MEDPS1, MNGIE	0,913074423	0,763925122
PDGF-BB	18591		1,159764374	0,661286817
Pentraxin 2/SAP	20219	PTX2	0,725538398	0,476010065
Pentraxin 3/TSG-14	19288	PTX3	0,180856364	0,020913325
Periostin/OSF-2	50706	Fasciclin I-like, POSTN, TRIF52	0,021020125	0,002427582
Pref-1/DLK-1/FA1	13386	DLK1, pG2, ZOG	0,394640438	0,137997571
Proliferin	18811	MRP	0,584610541	0,292058903
Proprotein Convertase 9/PCSK9	100102	NARC-1	0,50481111	0,28189703
RAGE	11596	AGER	0,978195585	0,929252222
RBP4	19662	Retinol-Binding Protein 4	0,256795169	0,024252989
Reg3G	19695	PAP3	1,72852729	0,7281997
Resistin	57264	ADSF, FIZZ3	2,018125422	0,384938916
Serpin E1/PAI-1	18787	Nexin, PLANH1	1,014533681	0,934641044
Serpin F1/PEDF	20317	EPC-1	0,778689666	0,61665454
Thrombopoietin	21832	Tpo, MGDF	0,822966879	0,61665454
TIM-1/KIM-1/HAVCR	171283		0,815316176	0,61665454
TNF-alpha	21926	TNFSF1A	1,104257213	0,744702849
VCAM-1/CD106	22329		0,517483341	0,186640699
VEGF	22339	VEGF-A, VPF	1,742765277	0,074510558
WISP-1/CCN4	22402		1,614596917	0,055666011

Table S2B : Relative cytokine production levels in *pml*$^{-/-}$ versus *pml*$^{+/+}$ MEFs after infection with a Δ*hly Listeria* mutant.

Cytokine production was quantified using supernatants from *pml*$^{-/-}$ and *pml*$^{+/+}$ MEFs infected for 24 h with a Δ*hly Listeria* mutant. Data represent fold changes of cytokine production levels in *pml*$^{-/-}$ MEFs compared to the levels in *pml*$^{+/+}$ MEFs (mean results from 3 independent experiments). Cytokines that had fold changes with an adjusted *P* value of <0.05 (Benjamini and Hochberg method) are considered differentially produced between the two conditions being compared.

Description	Entrez Gene ID	Alternative nomenclature	fold change	adj. p-value
Adiponectin/Acrp30	11450	AdipoQ	0,829764455	0,691219546
Amphiregulin	11839	AR, SDGF	1,042141762	0,949448374
Angiopoietin-1	11600	Ang-1, Angpt1	0,475464001	0,047058867
Angiopoietin-2	11601	Ang-2, Angpt2	0,852499588	0,575748602
Angiopoietin-like 3	30924	ANGPT-L3	0,655276632	0,226134458
BAFF/BLyS/TNFSF13B	24099	CD257, TALL1, THANK, ZTNF4	0,376942326	0,018953586
C-reactive Protein/CRP	12944		0,289058517	0,252136889
C1qR1/CD93	17064	AA4, Antigen C1qRp, CD93	0,72975292	0,352917165
CCL11/Eotaxin	20292		0,77264423	0,365512544
CCL12/MCP-5	20293		1,192034005	0,736532987
CCL17/TARC	20295		1,043199413	0,94138404
CCL19/MIP-3beta	24047	ELC	0,714189101	0,235407209
CCL2/JE/MCP-1	20296	MCAF	0,862569133	0,529838851
CCL20/MIP-3alpha	20297	exodus-1, LARC	0,175427093	0,156761026
CCL21/6Ckine	18829	exodus-2, SCYA21, SLC, TCA-4	0,78028837	0,531377891
CCL22/MDC	20299	ABCD-1, MDC, STCP-1	0,692413464	0,365512544
CCL3/CCL4/MIP-1alpha/beta	20302/20303		1,199020411	0,637583399
CCL5/RANTES	20304	SISd	0,80138872	0,424550881
CCL6/C10	20305	MRP-1	1,073439043	0,876962795
CD14	12475		0,667186403	0,711112004
CD160	54215	Natural killer cell receptor BY55, NK1, NK28	0,837620199	0,731496082
CD40/TNFRSF5	21939		0,968031589	0,967720307
Chemerin	71660	RARRES2, TIG-2	1,017533696	0,949448374
Chitinase 3-like 1	12654	CHI3L1, Cgp39, YKL40	0,100021572	0,015210621
Coagulation Factor III/Tissue Factor	14066	TF, CD142, Thromboplastin	0,372837215	0,013290592
Complement component C5/C5a	15139	C5/C5a	0,687318572	0,295812405
Complement Factor D	11537	Adipsin, C3 convertase activator, Properdin factor D	0,241286967	9,84E-02
CX3CL1/Fractalkine	20312	FKN, Neurotactin	0,708701467	0,235893617
CXCL1/KC	14825	CINC-1, GRO alpha, KC, MGSA-alpha	0,651026636	0,252136889
CXCL10/IP-10	15945	CRG-2, C7	0,57317212	0,199796565
CXCL11/I-TAC	56066	H174, SCYB9B	0,1489732	0,193830578
CXCL13/BLC/BCA-1	55985		0,743733094	0,442206224
CXCL16	66102	SRPSOX	0,385827886	0,151200279
CXCL2/MIP-2	20310	GRO beta	0,354043867	0,424550881
CXCL9/MIG	17329	CRG-10	0,801761256	0,575748602
Cystatin C	13010	ARMD11, CST3, Gamma-trae-ce	0,773470348	0,256222236
DKK-1	13380	Dickkopf-1	0,422485635	0,020793906
DPPIV/CD26	13482	Dpp4, Dipeptidyl-peptidase IV	0,679389303	0,278730829
E-Selectin/CD62E	20339	ELAM1, LECAM2, Sele	1,182493705	0,711112004
EGF	13645	Epidermal Growth Factor	0,949714449	0,854491865
Endoglin/CD105	13805	ENG	0,572920615	0,226134458
Endostatin	12822	Col18a1	0,330222741	0,013290592
Fetuin A/AHSG	11625	AHSG, alpha-2-HS-glycoprotein	0,537506747	0,193830578
FGF acidic	14164	FGF-1	0,603225364	2,90E-01
FGF-21	56636		0,774367053	0,711112004
Flt-3 Ligand	14256	Flt3lg	1,865208578	0,252136889
G-CSF	12985	Csf3	0,39684248	0,018239114
Gas 6	14456	Growth Arrest Specific	0,629973952	0,295812405
GDF-15	23886	MIC-1	0,712859099	0,321480879
GM-CSF	12981	Csf2	0,426903825	0,477755651
HGF	15234	Scatter Factor, SF, Hepatopoietin-A	1,175577187	0,711112004
ICAM-1/CD54	15894		0,977654743	0,949448374
IFN-gamma	15978	IFNG	0,731766093	0,404816152
IGFBP-1	16006		0,806677059	0,826521509
IGFBP-2	16008		0,022047338	0,000164315
IGFBP-3	16009		1,277817548	0,679195412
IGFBP-5	16011		0,583958963	0,252136889
IGFBP-6	16012		0,124678961	0,018239114
IL-10	16153	CSIF	1,287275576	0,510531542
IL-11	16156		1,033638816	0,949448374
IL-12p40	16160		0,647030872	0,193830578
IL-13	16163		1,115351089	0,736532987
IL-15	16168		0,820047131	0,637583399
IL-17A	16171		0,579694432	0,770882859
IL-1alpha/IL-1F1	16175		0,73564174	0,252136889
IL-1beta/IL-1F2	16176		0,905123998	0,696797623
IL-1ra/IL-1F3	16181	IL1RN	0,708925705	0,156761026
IL-2	16183		0,234922425	0,252136889
IL-22	50929	IL-TIF	1,252392351	0,531377891
IL-23	83430		1,121252936	0,711112004
IL-27p28	246779		0,852587145	0,711112004
IL-28A/B	330496/338374		0,640375739	0,193830578
IL-3	16187		0,719463533	0,682738544
IL-33	77125	NF HEV, DVS 27	0,666317431	0,352802271
IL-4	16189	B cell-stimulatory factor-1	0,740461097	0,252136889
IL-5	16191		0,924234292	0,83193417

IL-6	16193		0,149987577	0,193830578
IL-7	16196		0,833337607	0,679195412
LDL R	16835	low density lipoprotein receptor	1,183432526	0,766275704
Leptin	16846	OB	0,767599722	0,365512544
LIF	16878		0,414522819	0,083628888
Lipocalin-2/NGAL	16819	Siderocalin, 24p3	0,189135495	0,193830578
LIX	20311	CXCL5, GCP-2, ENA-78	0,259412573	0,252136889
M-CSF	12977	CSF-1	0,939175797	0,865863041
MMP-2	17390	Gelatinase A	0,571720018	0,235407209
MMP-3	17392	Stromelysin-1	0,005974972	9,80555E-06
MMP-9	17395	Clg4b, Gelatinase B, GELB	0,117617828	0,003276688
Myeloperoxidase	17523	MPO	1,248230532	0,711112004
Osteopontin (OPN)	20750	Eta-1, Spp1	0,989269102	0,966415423
Osteoprotegerin/TNFRSF11B	18383	OPG, Ocif	1,104270154	0,841692305
P-Selectin/CD62P	20344	GMP-140, LECAM3, Selep	1,208616939	0,682738544
PD-ECGF/Thymidine phosphorylase	72962	dThdPase, ECGF1, Gliostatin, MEDPS1, MNGIE	1,103916379	0,731496082
PDGF-BB	18591		0,906925968	0,736532987
Pentraxin 2/SAP	20219	PTX2	0,877721057	0,736532987
Pentraxin 3/TSG-14	19288	PTX3	0,254442008	0,03193414
Periostin/OSF-2	50706	Fasciclin I-like, POSTN, TRIF52	0,02220705	0,002694231
Pref-1/DLK-1/FA1	13386	DLK1, pG2, ZOG	0,443032531	0,225952956
Proliferin	18811	MRP	0,507559334	0,193830578
Proprotein Convertase 9/PCSK9	100102	NARC-1	0,680845827	0,531377891
RAGE	11596	AGER	1,102884929	0,736532987
RBP4	19662	Retinol-Binding Protein 4	0,27549925	0,021183112
Reg3G	19695	PAP3	0,819894777	0,902806381
Resistin	57264	ADSF, FIZZ3	1,330600404	0,711112004
Serpin E1/PAI-1	18787	Nexin, PLANH1	1,052076498	0,846155443
Serpin F1/PEDF	20317	EPC-1	0,730789813	0,485887501
Thrombopoietin	21832	Tpo, MGDF	0,854443721	0,682738544
TIM-1/KIM-1/HAVCR	171283		0,982288285	0,949448374
TNF-alpha	21926	TNFSF1A	0,731062714	0,256222236
VCAM-1/CD106	22329		0,671318424	0,424550881
VEGF	22339	VEGF-A, VPF	2,049083758	0,027139702
WISP-1/CCN4	22402		1,987990457	0,013290592

Table S3 : Relative gene expression levels in *pml*$^{+/+}$ MEFs treated or not with LLO.

Gene expression was determined by qPCR analysis of RNAs from *pml*$^{+/+}$ MEFs treated or not with 3 nM LLO for 30 min. Data represent fold changes of gene expression levels in LLO-treated versus untreated *pml*$^{+/+}$ MEFs (mean results from 3 independent experiments). Genes that had fold changes with an adjusted *P* value of >0.05 (Benjamini and Hochberg method) are considered not differentially regulated between the two conditions being compared.

Symbol	Unigene	Refseq	Description	fold change	adj. p-value
Akt1	Mm.6645	NM_009652	Thymoma viral proto-oncogene 1	1,089856447	0,912246957
Apcs	Mm.330510	NM_011318	Serum amyloid P-component	0,941258511	0,912246957
Birc3	Mm.2026	NM_007464	Baculoviral IAP repeat-containing 3	0,926254342	0,912246957
Bpi	Mm.260883	NM_177850	Bactericidal permeablility increasing protein	0,95067172	0,9373416
Camp	Mm.3834	NM_009921	Cathelicidin antimicrobial peptide	0,722835941	0,912246957
Card6	Mm.31252	NM_001163138	Caspase recruitment domain family, member 6	1,191758158	0,912246957
Card9	Mm.330064	NM_001037747	Caspase recruitment domain family, member 9	0,725390614	0,912246957
Casp1	Mm.1051	NM_009807	Caspase 1	0,941258511	0,912246957
Casp8	Mm.336851	NM_009812	Caspase 8	1,258733875	0,912246957
Ccl3	Mm.1282	NM_011337	Chemokine (C-C motif) ligand 3	0,941258511	0,912246957
Ccl4	Mm.244263	NM_013652	Chemokine (C-C motif) ligand 4	1,059018521	0,956218753
Ccl5	Mm.284248	NM_013653	Chemokine (C-C motif) ligand 5	1,184121971	0,912246957
Cd14	Mm.3460	NM_009841	CD14 antigen	0,711014065	0,909919813
Chuk	Mm.3996	NM_007700	Conserved helix-loop-helix ubiquitous kinase	1,009603846	0,956706977
Crp	Mm.28767	NM_007768	C-reactive protein, pentraxin-related	0,941258511	0,912246957
Ctsg	Mm.4858	NM_007800	Cathepsin G	0,941258511	0,912246957
Cxcl1	Mm.21013	NM_008176	Chemokine (C-X-C motif) ligand 1	1,94416922	0,912246957
Cxcl3	Mm.244289	NM_203320	Chemokine (C-X-C motif) ligand 3	0,740701754	0,912246957
Dmbt1	Mm.4138	NM_007769	Deleted in malignant brain tumors 1	0,941258511	0,912246957
Fadd	Mm.5126	NM_010175	Fas (TNFRSF6)-associated via death domain	0,846236476	0,912246957
Hsp90aa1	Mm.1843	NM_010480	Heat shock protein 90, alpha (cytosolic), class A member 1	1,167481011	0,912246957
Ifna9	Mm.377092	NM_010507	Interferon alpha 9	0,167482115	0,912246957
Ifnb1	Mm.1245	NM_010510	Interferon beta 1, fibroblast	1,148359945	0,912246957
Ikbkb	Mm.277886	NM_010546	Inhibitor of kappaB kinase beta	1,000366973	0,997448679
Il12a	Mm.103783	NM_008351	Interleukin 12A	0,941258511	0,912246957
Il12b	Mm.239707	NM_008352	Interleukin 12B	0,941258511	0,912246957
Il18	Mm.1410	NM_008360	Interleukin 18	0,804722942	9,12E-01
Il1b	Mm.222830	NM_008361	Interleukin 1 beta	0,941258511	0,912246957
Il6	Mm.1019	NM_031168	Interleukin 6	0,683220493	0,912246957
Irak1	Mm.38241	NM_008363	Interleukin-1 receptor-associated kinase 1	0,883259909	0,912246957
Irak3	Mm.146194	NM_028679	Interleukin-1 receptor-associated kinase 3	0,808111749	0,912246957
Irf5	Mm.6479	NM_012057	Interferon regulatory factor 5	1,117710805	0,912246957
Irf7	Mm.3233	NM_016850	Interferon regulatory factor 7	0,953385386	0,956218753
Jun	Mm.275071	NM_010591	Jun oncogene	3,817951999	0,13278976
Lbp	Mm.218846	NM_008489	Lipopolysaccharide binding protein	0,869330861	0,912246957
Lcn2	Mm.9537	NM_008491	Lipocalin 2	1,491920218	0,912246957
Ltf	Mm.282359	NM_008522	Lactotransferrin	0,941258511	0,912246957
Ly96	Mm.116844	NM_016923	Lymphocyte antigen 96	0,873575669	0,912246957
Lyz2	Mm.45436	NM_017372	Lysozyme 2	0,96785926	0,956218753
Map2k1	Mm.248907	NM_008927	Mitogen-activated protein kinase kinase 1	1,01067251	0,956706977
Map2k3	Mm.18494	NM_008928	Mitogen-activated protein kinase kinase 3	1,009413366	0,956706977
Map2k4	Mm.412922	NM_009157	Mitogen-activated protein kinase kinase 4	1,088841458	0,912246957
Map3k7	Mm.258589	NM_172688	Mitogen-activated protein kinase kinase kinase 7	0,825178632	0,912246957
Mapk1	Mm.196581	NM_011949	Mitogen-activated protein kinase 1	0,964696812	0,9373416
Mapk14	Mm.311337	NM_011951	Mitogen-activated protein kinase 14	0,923816346	0,912246957
Mapk3	Mm.8385	NM_011952	Mitogen-activated protein kinase 3	0,9226494	0,912246957
Mapk8	Mm.21495	NM_016700	Mitogen-activated protein kinase 8	1,078532991	0,912246957
Mefv	Mm.143718	NM_019453	Mediterranean fever	0,941258511	0,912246957
Mpo	Mm.4668	NM_010824	Myeloperoxidase	0,941258511	9,12E-01
Myd88	Mm.213003	NM_010851	Myeloid differentiation primary response gene 88	0,806541768	0,912246957
Naip1	Mm.6898	NM_008670	NLR family, apoptosis inhibitory protein 1	0,941258511	0,912246957
Nfkb1	Mm.256765	NM_008689	Nuclear factor of kappa light polypeptide gene enhancer in B-cells 1, p105	0,949879038	0,912246957
Nfkbia	Mm.170515	NM_010907	Nuclear factor of kappa light polypeptide gene enhancer in B-cells inhibitor, alpha	1,202547154	0,912246957
Nlrc4	Mm.311884	NM_001033367	NLR family, CARD domain containing 4	0,970923773	0,956218753
Nlrp1a	Mm.240227	NM_001004142	NLR family, pyrin domain containing 1A	0,941258511	0,912246957
Nlrp3	Mm.54174	NM_145827	NLR family, pyrin domain containing 3	0,941258511	0,912246957
Nod1	Mm.28498	NM_172729	Nucleotide-binding oligomerization domain containing 1	0,837088403	0,912246957
Nod2	Mm.222633	NM_145857	Nucleotide-binding oligomerization domain containing 2	0,581817399	0,909919813
Pik3ca	Mm.260521	NM_008839	Phosphatidylinositol 3-kinase, catalytic, alpha polypeptide	1,011628314	0,956706977
Prtn3	Mm.2364	NM_011178	Proteinase 3	0,941258511	0,912246957
Pstpip1	Mm.2534	NM_011193	Proline-serine-threonine phosphatase-interacting protein 1	0,836516131	0,912246957
Pycard	Mm.24163	NM_023258	PYD and CARD domain containing	0,661231547	0,912246957
Rac1	Mm.292510	NM_009007	RAS-related C3 botulinum substrate 1	0,944479623	0,912246957
Rela	Mm.249966	NM_009045	V-rel reticuloendotheliosis viral oncogene homolog A (avian)	0,903626908	0,912246957
Ripk1	Mm.374799	NM_009068	Receptor (TNFRSF)-interacting serine-threonine kinase 1	0,855174772	0,912246957
Ripk2	Mm.112765	NM_138952	Receptor (TNFRSF)-interacting serine-threonine kinase 2	0,979070778	0,956218753
Slc11a1	Mm.2913	NM_013612	Solute carrier family 11 (proton-coupled divalent metal ion transporters), member 1	1,127561464	0,912246957
Slpi	Mm.371583	NM_011414	Secretory leukocyte peptidase inhibitor	1,131220898	0,912246957
Sugt1	Mm.18972	NM_026474	SGT1, suppressor of G2 allele of SKP1 (S. cerevisiae)	0,948251582	0,912246957
Ticam1	Mm.203952	NM_174989	Toll-like receptor adaptor molecule 1	0,823704854	0,912246957
Ticam2	Mm.149280	NM_173394	Toll-like receptor adaptor molecule 2	0,675110736	0,912246957
Tirap	Mm.23987	NM_054096	Toll-interleukin 1 receptor (TIR) domain-containing adaptor protein	0,799476325	0,912246957
Tlr1	Mm.273024	NM_030682	Toll-like receptor 1	0,7490875	0,912246957
Tlr2	Mm.87596	NM_011905	Toll-like receptor 2	0,788837762	0,912246957
Tlr4	Mm.38049	NM_021297	Toll-like receptor 4	0,749323137	0,912246957
Tlr5	Mm.116894	NM_016928	Toll-like receptor 5	0,658911828	0,912246957
Tlr6	Mm.42146	NM_011604	Toll-like receptor 6	1,208099425	0,956218753

Tlr9	Mm.44889	NM_031178	Toll-like receptor 9	0,941258511	0,912246957
Tnf	Mm.1293	NM_013693	Tumor necrosis factor	0,941258511	0,912246957
Tnfrsf1a	Mm.1258	NM_011609	Tumor necrosis factor receptor superfamily, member 1a	0,958102144	0,956218753
Tollip	Mm.103551	NM_023764	Toll interacting protein	1,08202457	0,912246957
Traf6	Mm.292729	NM_009424	Tnf receptor-associated factor 6	0,943299328	0,912246957
Xiap	Mm.259879	NM_009688	X-linked inhibitor of apoptosis	0,859679023	0,912246957
Zbp1	Mm.116687	NM_021394	Z-DNA binding protein 1	1,112438185	0,956218753
Actb	Mm.328431	NM_007393	Actin, beta	0,948936184	0,912246957
B2m	Mm.163	NM_009735	Beta-2 microglobulin	0,959446023	0,912246957
Gapdh	Mm.309092	NM_008084	Glyceraldehyde-3-phosphate dehydrogenase	0,985682857	0,956218753
Gusb	Mm.3317	NM_010368	Glucuronidase, beta	1,081756852	0,912246957
Hsp90ab1	Mm.2180	NM_008302	Heat shock protein 90 alpha (cytosolic), class B member 1	1,030089976	0,956218753

Supplementary Table S4 : Primary antibody information.

Targeted Protein	Assay (dilution)	Species	Source	Reference
Actin	WB (1:10,000)	Mouse	Sigma-Aldrich	R5441
Ubc9	WB (1:1,000)	Mouse	BD Biosciences	610748
K48-linked polyubiquitin	WB (1:1,000)	Rabbit	Cell Signaling Technology	D9D5; #8081
LLO	WB (1:20,000)	Rabbit	Home-made	R176
PML	WB (1:2,000)	Chicken	Home-made	
PML	IF (1:500)	Mouse	Home-made	2'C7
Sp100	WB (1:2,000)	Rabbit	Home-made	
SUMO1	WB (1:1,000)	Rabbit	Home-made	R204 (p)
SUMO1	IF (1:100)	Rabbit	Cell Signaling Technology	#4930
SUMO3	WB (1:5,000)	Rabbit	Home-made	R205 (is2)
SUMO3	IF (1:500)	Rabbit	Home-made	R206 (p)
Lamin B	IF (1:200) WB (1:1,000)	Goat	Santa Cruz Biotechnology	M-20; sc-6217
RXRα	IF (1:200)	Rabbit	Santa Cruz Biotechnology	D-20; sc-553
FLAG	WB (1:1,000) IF (1:200)	Mouse	Sigma-Aldrich	M2; F3165
FLAG	IF (1:200)	Rabbit	Sigma-Aldrich	F7425